Journal of Translational Medicine

RESEARCH

Open Access

Human neural stem cell-derived exosomes activate PINK1/Parkin pathway to protect against oxidative stress-induced neuronal injury in ischemic stroke

Mengke Zhao[1,2,3,4†], Jiayi Wang[1,2,3,4†], Shuaiyu Zhu[1,2,3,4], Shensen Zhang[1,2,3,4], Chao Han[1,2,3,4], Chengcheng Tan[1,2,3,4], Yubing Huang[1,2,3,4], Zhaokai Sun[1,2,3,4], Liang Wang[1,2,3,4*] and Jing Liu[1,2,3,4*]

Abstract

Background Mitochondria play a critical role in oxidative stress (OS)-induced neuronal injury during ischemic stroke (IS), making them promising therapeutic targets. Mounting evidence underscores the extraordinary therapeutic promise of exosomes derived from human neural stem cells (hNSCs) in the management of central nervous system (CNS) diseases. Nonetheless, the precise mechanisms by which these exosomes target mitochondria to ameliorate the effects of IS remain only partially elucidated. This study investigates the protective effects of hNSC derived exosomes (hNSC-Exos) on neuronal damage.

Methods Using a rat model of middle cerebral artery occlusion (MCAO) in vivo and OS-induced HT22 cells in vitro. Firstly, our research group independently isolated human neural stem cells (hNSCs) and subsequently prepared hNSC-Exos. In vivo, MCAO rats were restored to blood flow perfusion to simulate ischemia–reperfusion injury, and hNSC-Exos were injected through stereotaxic injection into the brain. Subsequently, the protective effects of hNSC-Exos on MCAO rats were evaluated, including histological studies, behavioral assessments. In vivo, H_2O_2 was used in HT22 cells to simulate the OS environment in MCAO, and then its protective effects on HT22 were evaluated by co-culturing with hNSC-Exos, including immunofluorescence staining, western blotting (WB), quantitative real time PCR (qRT-PCR). In the process of exploring specific mechanisms, we utilized RNA sequencing (RNA-seq) to detect the potential induction of mitophagy in OS-induced HT22 cells. Afterwards, we employed a series of mitochondrial function assessments and autophagy related detection techniques, including measuring mitochondrial membrane potential, reactive oxygen species (ROS) levels, transmission electron microscopy (TEM) imaging, monodansylcadaverine (MDC) staining, and mCherry-GFP-LC3B staining. In addition, we further investigated the regulatory pathway of hNSC-Exos by using autophagy inhibitor mdivi-1 and knocking out PTEN induced kinase 1 (PINK1) in HT22 cells.

Results Administration of hNSC-Exos significantly ameliorated brain tissue damage and enhanced behavioral outcomes in MCAO rats. This treatment led to a reduction in brain tissue apoptosis and facilitated the normalization of impaired neurogenesis and neuroplasticity. Notably, the application of hNSC-Exos in vitro resulted

†Mengke Zhao and Jiayi Wang contributed equally to this work.

*Correspondence:
Liang Wang
wangliang@dmu.edu.cn
Jing Liu
liujing@dmu.edu.cn
Full list of author information is available at the end of the article

in an upregulation of mitophagy in HT22 cells, thereby remedying mitochondrial dysfunction. We demonstrate that hNSC-Exos activate mitophagy via the PINK1/Parkin pathway, improving mitochondrial function and reducing neuronal apoptosis.

Conclusions These findings suggest that hNSC-Exos alleviate OS-induced neuronal damage by regulating the PINK1/Parkin pathway. These reveals a novel role of stem cell-derived mitochondrial therapy in promoting neuroprotection and suggest their potential as a therapeutic approach for OS-associated CNS diseases, including IS.

Keywords Human neural stem cells, Exosomes, Mitophagy, PINK1/Parkin pathway, Oxidative stress, Neuroprotection, Ischemic stroke

Graphical Abstract

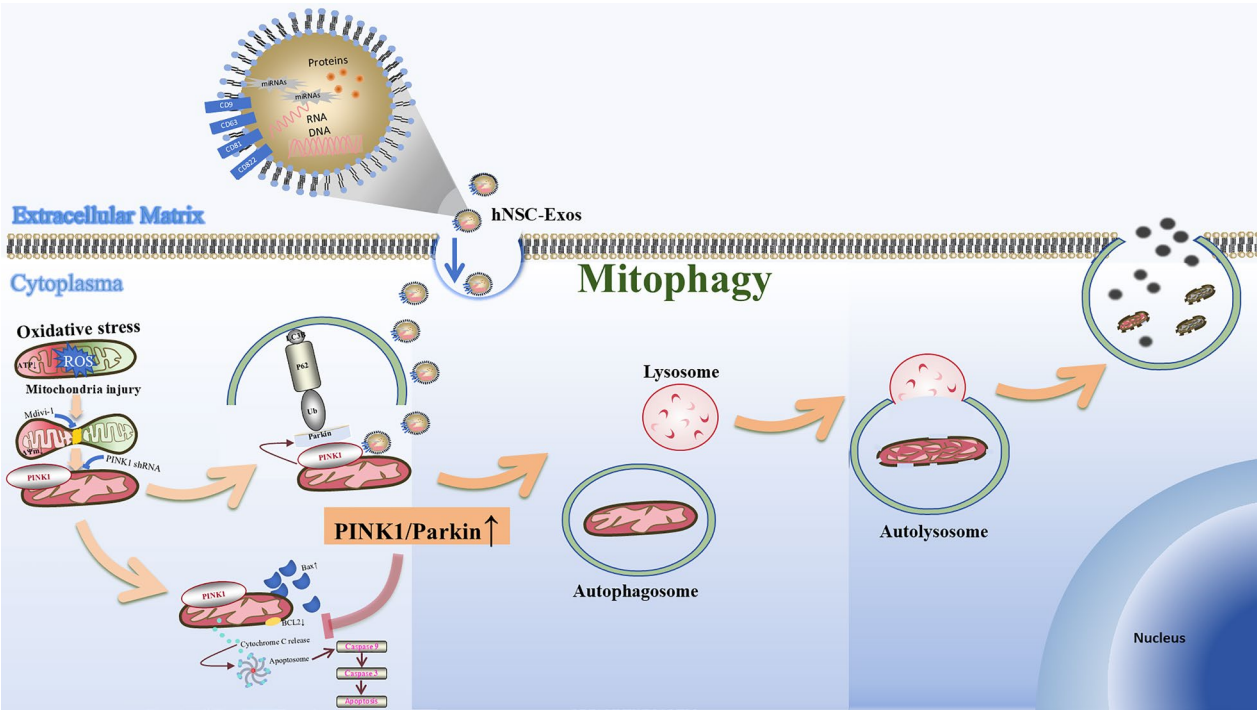

Background

Mitochondria are crucial for maintaining energy metabolism. Following the onset of ischemic stroke (IS), the lack of glucose and oxygen leads to significant impairment in mitochondrial structure and function [1]. During this process, the efficiency of electron transport is reduced, resulting in increased electron leakage and the generation of reactive oxygen species (ROS) such as superoxide anions [2]. This triggers oxidative stress (OS), which damages DNA, RNA, proteins, and lipid peroxidation, further disrupting mitochondrial integrity. In the cerebral ischemia/reperfusion injury (CIRI) phase, the restoration of oxygen causes a burst of ROS production, exacerbating mitochondrial damage and OS, which are key factors in the pathogenic cascade of IS. Among these, mitochondria-dependent apoptosis is one of the critical events following IS [3]. Therefore, drugs targeting the regulation of the mitochondrial microenvironment and enhancing antioxidant effects during ischemia are essential therapeutic strategies for stroke management [4]. While advancements in vascular recanalization and research on ischemic tissue damage have achieved some clinical success in IS treatment [5], there are currently no effective therapeutic strategies to prevent the secondary damage caused by OS during CIRI. Thus, the development of novel therapies targeting CIRI is urgently needed.

Stem cells, have garnered attention as naturally occurring bioactive entities for treating neurological disorders

such as IS through the regulation of mitochondrial bioenergetics. For example, neural stem cells (NSCs) reduced the expression of inflammatory factors and improved blood–brain barrier (BBB) damage [6, 7]. Mesenchymal stem cells (MSCs) reduced apoptosis and inflammation after stroke, and rescued damaged cerebral microvessels [8]. Embryonic stem cells (ESCs) improve brain neural repair [9]. Unlike stem cells from other sources, hNSCs closely resemble neural cells in morphology and function [10]. Their surface may express neuron-specific membrane proteins, enabling them to traverse the BBB and deliver tissue-specific neurotrophic and differentiation-inducing factors to injured brain regions, thereby promoting the recovery of brain structure and neurological function after ischemic injury [11]. While hNSCs have demonstrated significant potential in preclinical and clinical studies for various neurological diseases, challenges related to safety, stability, delivery efficiency, and multi-mechanistic synergy highlight the unique advantages of hNSC-derived exosomes (hNSC-Exos) as a novel therapeutic strategy [12]. hNSC-Exos, by delivering bioactive molecules (e.g., miRNAs, proteins, lipids), exhibit remarkable promise in neuroprotection, injury repair, and disease treatment for central nervous system (CNS) diseases, including Alzheimer's disease (AD) [13], Parkinson's disease (PD) [14], and traumatic brain injury (TBI) [15], offering a therapeutic approach to address OS-mediated mitochondrial dysfunction and potentially fill the current gap in CIRI treatment strategies [16]. However, critical challenges such as technical standardization, targeted delivery, and efficacy validation must be overcome during clinical translation. A deeper exploration of their mechanisms of action is essential to advance hNSC-Exos from laboratory research to clinical application.

Mitophagy is a critical mechanism that induces neuronal apoptosis in response to OS, selectively removing damaged or dysfunctional mitochondria through autophagy via lysosomes or peroxisomes [17–21]. Among the multiple signaling pathways that regulate mitophagy, including PTEN-induced kinase 1 (PINK1)/Parkin, MAPK/ERK/CREB, BNIP3, NIX, etc. [22, 23], the ubiquitin-dependent PINK1/Parkin pathway is the main signaling pathway controlling mitophagy [24]. This is because PINK1/Parkin has a highly sensitive damage response capability, a strong ubiquitination signal amplification effect, and evolutionary conservation, making it a key target for current research and therapeutic development [25]. This involves mitochondrial dynamics disrupted by OS-activated dynamin-related protein 1 (Drp1)-driven mitochondrial fission and oxidative optic atrophy type 1 protein (OPA1)-inhibited mitochondrial fusion [26–28]. The accumulation of fragmented mitochondria produced by excessive fission triggers the occurrence of mitophagy, regulating the dynamic balance between mitochondrial fusion and fission to alleviate OS-induced cell damage. PINK1, which depends on the stability of the mitochondrial membrane potential, cannot enter the inner mitochondrial membrane (IMM) and accumulates on the outer mitochondrial membrane (OMM) in various diseases [29]. This accumulation leads to triggering mitochondrial phagocytosis through the phosphorylation of ubiquitin and recruitment of E3 ligase Parkin [30]. Therefore, mitochondrial quality control through the mechanism of mitophagy has become a key target for therapeutic intervention in neurological diseases (such as IS, AD, and PD) and cardiovascular diseases (such as myocardial infarction), although it is specific due to differences in pathological background [31, 32]. For example, in IS, there is an acute compensatory mechanism that rapidly clears damaged mitochondria through mitophagy, whereas in other diseases, including AD or PD, the compensation is primarily characterized by chronic compensatory dysfunction. Exosomes derived from non-hNSCs have shown significant potential in neuroprotection, injury repair, and disease treatment through mitophagy, such as umbilical cord MSC-exosomes activating the PINK1/Parkin pathway to inhibit programmed cell death in TBI [33], while extracellular vesicles from adipose derived stem cells regulate the BNIP3 pathway to alleviate mitochondrial oxidative damage in cardiomyocytes [34]. As well as bone marrow derived exosomal miR-143-3p reduces apoptosis by regulating the CHK2-Beclin2 autophagy pathway [35]. As exosomes from stem cells that are more easily taken up by neurons, although hNSC-Exos are rich in miRNAs such as miR-30d and miR-21, proteins including HSP70 and MFN2, and lipids and metabolites like sphingomyelin and ATP/NAD^+ involved in neuroprotection. Although studies have reported that miR-30d targets autophagy-related proteins such as Beclin and Atg5 in brain injury models, there is relatively little research on the regulation of neuronal recovery by hNSC-Exos through autophagy [36]. This also prompted us to conduct an in-depth investigation.

Due to the crucial role of mitophagy in OS-induced neuronal apoptosis, here, we demonstrate that hNSC-Exos improve mitochondrial function and reduce neuronal apoptosis by promoting mitophagy. These findings reveal a novel role for hNSC-Exos in enhancing neuroprotection and indicate their potential as a therapeutic approach for OS-related CNS diseases, including IS.

Methods

Experimental animals

All 30 healthy adult male sprague dawley (SD) rats (male, 8–10-week-old, 250–280 g) were purchased from the Animal Experiment Center of Dalian Medical University. They were grouped and given a period of time to adapt to

the laboratory environment. All animal experiments were approved by the Ethics Committee of the Animal Experiment Center of Dalian Medical University and performed following the Guide for the Care and Use of Laboratory Animals of the National Institutes of Health (Ethical No. AEE23127, Feb. 28th 2023). They were housed in a specific-pathogen-free animal central laboratory with 50% relative humidity, 22 ± 2 °C temperature, and a 12-h light and dark cycle. They were free to consume standard rat food and water. The animals were excluded if the animal died prematurely, preventing the collection of behavioral and histological data. At the end of the observation period, the rats were humanely euthanized with carbon dioxide in accordance with the institutional guidelines. All animal experiments were reported in line with the ARRIVE guidelines (Animal Research: Reporting of In Vivo Experiments).

Cell culture and treatment

Mouse hippocampal neurons

Mouse hippocampal neurons (HT22; RRID: CVCL_0321) were provided by the Laboratory of Dalian Medical University. Considering that neurons are more susceptible to OS and have higher metabolic demands, HT22 cells were chosen as the in vitro research subject in this study. HT22 cells were cultured in dulbecco's modified eagle medium (DMEM) high-glucose medium (MeilunBio, MA0560, Dalian, China), fetal bovine serum, penicillin and streptomycin. HT22 cells were cultured in an incubator at 37 °C with 5% CO_2. They were subcultured at 3-day intervals and carried out using passages 4–8. An OS-induced cell injury model was established by treating HT22 cells with H_2O_2 (400 μM, Sigma-aldrich, HX0640, Darmstadt, Germany) for 6 h in vitro. And the "Mdivi-1" group comprises HT22 cells exposed to 400 μM H_2O_2 while also being treated with the mitophagy inhibitor 10 μM mdivi-1 (MedChemExpress, HY015886, New Jersey, USA) in vitro. The concentrations of H_2O_2 and mdivi-1 were referenced from previously published literature [28, 37] and it has been confirmed in this study that the essence of this model is apoptosis caused by OS and inhibition of the mitophagy pathway.

hNSCs

This study was approved by the Clinical Research Ethics Committee of the First Affiliated Hospital of Dalian Medical University (Ethical No. LCKY2016-60, Dec. 2nd 2016). hNSCs were isolated from the human fetal forebrain tissue of healthy pregnant women at 10–12 weeks of gestation who requested induced abortion, all of whom provided informed consent. Our research group has independently established a seed bank for NSCs. And the tests for human immunodeficiency virus, syphilis, hepatitis B, and other pathogenic microorganisms were negative, as we previously reported [38]. The extraction method of hNSCs was as described earlier. Within 6 h after miscarriage, the forebrain tissue isolated from the aborted fetus was transported by cold chain to our research group's stem cell preparation center, which has been registered with the China Food and Drug Administration. hNSCs were extracted strictly according to the established protocol in our laboratory. hNSC basal medium (Stemcell Technologies, 05751, Vancouver, Canada), epidermal growth factor (Stemcell Technologies, 78,136.1 l, Vancouver, Canada), basic fibroblast growth factor (Stemcell Technologies, 78,134.1, Vancouver, Canada), heparin (Stemcell Technologies, 07980, Vancouver, Canada), penicillin and streptomycin (Solarbio, P1400, Beijing, China) were used to culture the qualified hNSCs. hNSCs were cultured in adherent flasks coated with matrigel (Corning, 356,234, New York, USA). Cells were cultured in an incubator (Escolifesciences, IFC-240, Singapore) at 37 °C with 5% CO_2. The hNSCs were subcultured at 3-day intervals and carried out using passages 4–8. We strictly controlled the quality of hNSCs during passage by monitoring cell viability and marker expression.

hNSC-Exos isolation

The ultracentrifugation was employed to purify the exosomes. hNSCs were cultured for 3-day by exo-free FBS cell culture medium, the cell supernatant was collected and transferred to a centrifuge tube (Sparkjade, GD0001, Jinan, China). Repeated gradient centrifugation was performed at 200 g for 10 min, 2,000 g for 20 min, and 20,000 g for 30 min. The supernatant was collected, filtered through a 0.22-μm sterile filter (Merck, SLGPR33RB, California, USA), and added to an ultracentrifuge (Beckman, Optima XPN-100, Brea, USA). After centrifugation at 100,000 g and 4 °C for 1.5 h, the precipitate was resuspended in a little sterile phosphate buffered saline (PBS) (MeilunBio, MA0015, Dalian, China) and quantified in aliquots. The obtained-exosomes were quantified using bicinchoninic acid reaction kit (Thermo Fisher Scientific, 23,227, Massachusetts, USA). In this study, the density of hNSC-Exos was 1–1.2 g/ml, and they were divided into 40 μg/tube according to experimental requirements. Before storage, quality control was carried out by detecting particle size through Nanoparticle tracking analysis (NTA) and protein integrity through western blotting (WB). Once the control standards were met, the samples were quickly frozen at -80 ℃ to avoid multiple thawing cycles. In vitro, hNSC-Exos precipitates were resuspended in fresh medium at 40 μg/ml and experiments were performed at 20 μg/group. hNSC-Exos were co-cultured with OS-induced HT22 for 6 h. In vivo,

hNSC-Exos precipitates were resuspended in 7 μg/μL of hNSC-Exos dissolved in 10 μL of PBS. The therapeutic concentration of hNSC-Exos selected in this study was based previous literature published by our research group [39].

NTA

hNSC-Exos were diluted 40 times with sterile PBS and then filtered with 0.22 μm sterile filter. The diameter and potential of exosomes were measured by ZetaView (Particle Metrix, PMX-120-Z, Munich, Germany). Data were analyzed using the ZetaView software 8.02.31. The particle size is mostly concentrated in 50–150 nm, with a main peak of about 80–120 nm and a negative potential.

Transmission electron microscopy (TEM)

TEM (Philips, TECNAI 20, Eindhoven, Netherlands) was used to observe the ultramorphology of the hNSC-Exos. After cleaning, the hNSC-Exos were fixed with 2% osmotic acid solution, dehydrated with a gradient of ethanol, mixed with acetone, immersed in an embedding plate for polymerization, and finally stained with uranyl acetate solution for observation. The TEM parameters are set to an acceleration voltage of 80–100 kV, an objective aperture of 20–30 μm, and an exposure time of 0.5–1 s. The complete hNSC-Exos are cup-shaped or double concave disc-shaped.

In addition, TEM was used to observe the mitochondrial morphology and autophagy structure of neurons in vitro. In vitro, hNSC-Exos were co-cultured with OS-induced HT22 for 6 h. After collecting HT22 cells, the above operation method was repeated. After fixation and dehydration treatment, the mitochondria were embedded and sliced to expose them in the observation field, and finally stained. The TEM parameters are set to an acceleration voltage of 80–120 kV, an objective aperture of 30–50 m, and an exposure time of 0.5–2 s. Normal mitochondria are elliptical or elongated in shape, with a diameter of about 0.5–1 μm and a length of 1–10 μm. They have a bilayer membrane structure and tightly arranged mitochondrial cristae. And the autophagosome is clearly visible as two membrane bilayers separated by electron translucent pores.

WB

Proteins were extracted from the cell, hNSC-Exos and animal models in each group using radio-immunoprecipitation assay lysis buffer (Thermo Fisher Scientific, 89,901, Massachusetts, USA) and quantified using a BCA kit (Thermo Fisher Scientific, 23,227, Massachusetts, USA). The protein samples were all normalized to the same concentration. Samples were added to a Bis–Tris preformed gel (Meilun, MA0445, Dalian, China) for electrophoresis using electrophoresis equipment (Life Technologies, EI0001, California, USA) set at 150 V and 600 mA for 1 h. Polyvinylidene fluoride membranes (Merck, IPFL00010, California, USA) were used for membrane transfer. A transfer solution (Meilun, MA0121, Dalian, China) was used, and the transfer conditions were set at 600 V and 300 mA for 1 h. Subsequently, they were blocked with skim milk (BD Difco, 232,100, Colombia, USA) and incubated overnight with primary antibodies, including CD9, CD63, CD81, TSG101, Calnexin, Bax, BCL2, Caspase 3, Cleaved caspase 3, Beclin, LC3B, Parkin, PINK1 and GAPDH. The next day, the membranes were then incubated at room temperature for 2 h with second antibodies. The bands were made visible through the use of an ECL kit (Thermo Fisher Scientific, 34,580, Massachusetts, USA) and chemiluminescence instrument (SuperSignal West Atto Supersensitive substrate, Thermo Fisher Scientific, A38554, Massachusetts, USA) were used for exposure development. Relative protein expression was normalized to that of GAPDH. ImageJ software was used to quantify the protein expression levels. The typical molecular weight range of hNSC-Exos marker proteins ranges from 25 to 95 kDa and the detailed information of all antibodies used is summarized in Table 1.

hNSC-Exos uptake

To determine the endocytosis of exosomes by hNSC-Exos which were initially labelled with the red fluorescent dye PKH26 (Sigma aldrich, MKCL4676, Darmstadt, Germany) concerning the manufacturer's instructions. In detail, after fluorescent labeling of hNSC-Exos with PKH26, hNSC-Exos rinsed with PBS were added to diluter C, and the mixture of PKH26 and diluter C was added to mix thoroughly. The reaction was terminated through serum addition, centrifuged (12,000 g, 4 °C, and 15 min), and washed several times with PBS before use. In vitro, PKH26-hNSC-Exos were co-cultured with HT22 for 6 h, and the cells were fixed, permeabilized, and incubated with actin-tracker green-488 (Beyotime, C2201S, Shanghai, China) for fluorescence staining of neuronal microfilaments. Subsequently, they were stained with 4′,6-diamidino-2-phenylindole (DAPI) (Solarbio, C0065, Beijing, China) and observed under a laser confocal microscope (Yokogawa, CV1000, Tokyo, Japan). In vivo, PKH26-hNSC-Exos were stereotaxically injected into the brain of middle cerebral artery occlusion (MCAO) rats during ischemia–reperfusion. After 24 h, the rats were sacrificed, and the brain tissues were frozen (Detailed operation approaches will be discussed later). Finally, the cells were stained with DAPI and observed under a laser confocal microscope.

Table 1 All antibodies and primer sequences for qPCR used in the manuscript

Antibody	Dilution rate	Supplier	Article number	Specific applications
CD9 Rabbit mAb	1:1000	Cell Stem Technology Massachusetts, USA	98,327	WB
CD63 Rabbit mAb	1:1000	Cell Stem Technology Massachusetts, USA	10,112	WB
CD81 Rabbit mAb	1:1000	Cell Stem Technology Massachusetts, USA	10,037	WB
TSG101 Rabbit mAb	1:1000	Cell Stem Technology Massachusetts, USA	72,312	WB
Calnexin Rabbit mAb	1:1000	Abcam Massachusetts, USA	Ab22595	WB
BCL2 Rabbit mAb	1:1000, 1:200	Abcam Massachusetts, USA	Ab182858	WB, Immunofluorescence staining
Caspase 3 Rabbit mAb	1:1000	Abcam Massachusetts, USA	Ab184787	WB
Cleaved caspase 3 Rabbit mAb	1:1000	Abcam Massachusetts, USA	Ab214430	WB
Beclin Rabbit mAb	1:1000, 1:100	Abcam Massachusetts, USA	Ab62557	WB,Immunofluorescence staining
LC3B Rabbit mAb	1:2000, 1:100	Abcam Massachusetts, USA	Ab192890	WB,Immunofluorescence staining
Parkin Rabbit mAb	1:1000	Cell Stem Technology Massachusetts, USA	2132	WB
PINK1 Rabbit mAb	1:1000, 1:500	Abcam Massachusetts, USA	Ab216144	WB,Immunofluorescence staining
GAPDH Rabbit mAb	1:1000	Cell Stem Technology Massachusetts, USA	2118	WB
Nestin Rabbit mAb	1:1000	Cell Stem Technology Massachusetts, USA	89,529	Immunofluorescence staining
SOX2 Rabbit mAb	1:400	Cell Stem Technology Massachusetts, USA	23,064	Immunofluorescence staining
Bax Rabbit mAb	1:1000, 1:200	Abcam Massachusetts, USA	Ab216494	Immunofluorescence staining
Anti-rabbit IgG, HRP-linked antibody	1:5000	Cell Stem Technology Massachusetts, USA	7074	WB
Anti-mouse IgG, HRP-linked antibody	1:5000	Cell Stem Technology Massachusetts, USA	7076	WB
Goat anti-mouse 647	1:500	Abcam Massachusetts, USA	Ab150115	Immunofluorescence staining
Goat anti-mouse 488	1:500	Abcam Massachusetts, USA	Ab150113	Immunofluorescence staining

qPCR Primer sequences

Gene	5′ to 3′ Forward Primer Sequence	5′ to 3′ Reverse Primer Sequence
Mm-Bax	TCAGGATGCGTCCACCAAGAAG	TGTGTCCACGGCGGCAATCATC
Mm-BCL2	ATCGCCCTGTGGATGACTGAGI	GCCAGGAGAAATCAAACAGAGAGGC
Mm- β-ctin	GATCAGATCTATTGCTCCTCCTG	ACGGGGCTCAGTACAGTCC

Flow cytometry

Carboxyfluorescein diacetate, succinimidyl ester (CFDA SE, Beyotime, C1031, Shanghai, China) was used to label the internalized hNSC-Exos. CFDA SE was prepared as a 5 μM working solution in anhydrous DMSO and mixed with hNSC-Exos, followed by incubation at room temperature. The labeling reaction was terminated by adding complete medium. The CFDA SE-labeled hNSC-Exos were co-cultured with HT22 cells for 6 h. Afterward, the cells were collected, resuspended in PBS, and analyzed by flow cytometry (Sony, SH800, Tokyo, Japan). If hNSC-Exos were not taken up by the cells, they were non-fluorescent. By comparing the cell sorting of hNSC-Exos that were co-cultured with cells to those that were not, we can determine whether hNSC-Exos had been internalized by the cells.

HT22 cell apoptosis was detected using a fluorescein isothiocyanate-Annexin V/PI apoptosis kit (Thermo Fisher Scientific, BMS500FI, Massachusetts, USA). We had set up three groups in vitro experiments, respectively. The "Control" group represents untreated HT22 cells, the "H_2O_2" group comprises HT22 cells exposed to 400 μM H_2O_2, and the "hNSC-Exos" group consists of HT22 cells exposed to 400 μM H_2O_2, followed by treatment with 20 μg hNSC-Exos. We ensured that each batch of cells in vitro was highly similar and randomly grouped, and this standard was maintained in subsequent experiments. After preparing the HT22 cell suspension, a

binding buffer was added, followed by the addition of fluorescent dye-coupled annexin V. The cells were incubated at 20 °C-25 °C for several minutes. A binding buffer was readded, and a propyl iodide staining solution was added. The cells were sorted using flow cytometry.

Cell viability assays

Cell viability of neurons was analyzed based on the inability of trypan blue (Thermo Fisher Scientific, T10282, Vancouver, USA) dye to penetrate the normal intact cell membrane of living cells. As described above, HT22 cells were treated. Cells were stained by trypan blue after treatment. Stained HT22 cells were considered non-viable, and unstained HT22 cells were considered viable. Cell survival rate = (Total cell count-Stained cell count) / Total cell count × 100%. Damaged cell rate = (Total cell count-Unstained cell count) / Total cell count × 100%. Statistical analysis of the three groups was performed to assess the cell survival and death rates of each group. Among them, the normal HT22 cells in the control group were not treated and were used as the negative control group.

In addition, a lactate dehydrogenase (LDH) release was used to indicate cytotoxicity and evaluated using an LDH cytotoxicity detection kit (DOJINDO, CK12, Tabaru, Japan). As described above, HT22 cells were treated. Cells were plated into a 96-well plate and various groups were treated with specific modeling techniques. Subsequently, 100 μL of the reaction mixture supplied with the kit was added to each well. The plate was then incubated under cell culture conditions at 37 °C with 5% CO_2 for 30 min. The optical density value at 490 nm using a microplate reader (DeTie, HBS-1096A, Nanjing, China). Statistical analysis of the three groups was performed to assess the cytotoxicity of each group (ImageJ, 1.52).

TdT-mediated dUTP nick end labeling (TUNEL) staining

The TUNEL apoptosis kit (Beyotime, C1090, Shanghai, China) was used to detect neuronal apoptosis in vitro and in vivo. Briefly, neuronal different groups in vitro and MCAO rat brain slices (frozen section manipulation methods are detailed later) were incubated with anti-NeuN antibodies (1:100, Abcam, Ab177487, Massachusetts, USA), and then incubated with a mixture of biotinylated dUTP catalyzed by dinitrotoluene and goat anti-rabbit 488 (1:500, Abcam, Ab150077, Massachusetts, USA) in the dark. An unlabeled solution was used as a negative control. Images were captured and photographed using a fluorescence microscope. The ratios of TUNEL-positive cells were calculated separately for randomly selected fields in different groups and images of representative areas by ImageJ.

Quantitative real time PCR (qRT-PCR)

qRT-PCR was performed to assess the gene expression in the experimental groups. Total RNA was extracted from the cell samples using the RNA extraction kit (QIAGEN, 21,017, Dusseldorf, Germany). The concentration and purity of RNA were assessed using a NanoDrop ND-1000 spectrophotometer (ThermoFisher Scientific, Waltham, USA). After extracting RNA, the reverse transcription kit (Accurate Biology, AG11728, Beijing, China) was utilized to perform reverse transcription, converting RNA into cDNA. qRT-PCR was performed on a real-time PCR machine (Bio-Rad, 1,855,200, California, USA) using a SYBR Green Pro Taq HS Premixed qPCR kit (Accurate Biology, AG11746, Beijing, China). Relative RNA expression levels were assessed using the $2^{-\triangle\triangle Ct}$ method. All the tests were performed in triplicate and β-actin was used as a genomic DNA control. qRT-PCR primers were purchased from Sangon Biotech (Shanghai, China) and the primer sequences are summarized in Table 1.

Immunofluorescence staining

HT22 cells and sections were fixed with 4% paraformaldehyde, permeabilized (Beyotime, China, P0096), blocked (Beyotime, P0260, Shanghai, China), and incubated with primary antibodies overnight, including Nestin, SOX2, Bax, BCL2, PINK1, Beclin, LC3B. The next day, they were treated with second antibodies and incubated for 1 h. DAPI was used to mark the nuclei. Images were captured by confocal microscopy using the same imaging threshold and exposure time for each experiment. The number of positive cells per field was calculated with ImageJ software. The detailed information of all antibodies used is summarized in Table 1.

Mitochondrial membrane potential and apoptosis detection

We used mitochondrial membrane potential and apoptosis detection kit with Mito-Tracker Red CMXRos and Annexin V-FITC (Beyotime, C1071, Shanghai, China) to detect mitochondrial membrane potential and apoptosis of HT22 cells. As described above, HT22 cells were treated. Following the manufacturer's instructions, the fluorescence was observed by fluorescence microscopy and analyzed by ImageJ. Red fluorescence marks viable cells that retain mitochondrial membrane potential, whereas green fluorescence marks cells that have undergone apoptosis or necrosis.

Intracellular ROS detection

The ROS assay kit-highly sensitive DCFH-DA (Dojindo, R252, Tabaru, Japan) was used to detect ROS production. After removing the medium, a high-sensitivity

DCFH-DA dye working solution was added after washing with Hank's Balanced Salt Solution (HBSS) (Beyotime, C0218, Shanghai, China). As described above, HT22 cells were treated. HT22 cells were cultured in an incubator for 30 min, rewashed with HBSS, and observed using fluorescence microscopy. The relative fluorescence intensity of DCFH was analyzed by ImageJ.

Mitochondrial reactive oxygen species (MtROS) detection

The MitoSOX Red probe (MedChemExpress, HY-D1055, New Jersey, USA) was used to detect mtROS production. As described above, HT22 cells were treated. After removing the medium, a MitoSOX Red working solution was added after washing with HBSS. HT22 cells were cultured in an incubator for 30 min, rewashed with HBSS, and observed using fluorescence microscopy. The relative fluorescence intensity was analyzed by ImageJ.

Malondialdehyde (MDA) detection

MDA detection kit (Beyotime, S0131S, Shanghai, China) was used to detect lipid oxidation levels. As described above, HT22 cells were treated. After treatment, the cells were washed with PBS and lysed. After centrifugation, the supernatant was collected for MDA detection. Following the manufacturer's instructions for MDA, the absorbance of cellular MDA at 532 nm was measured using an enzyme-labeled instrument, and the molar concentration of MDA was calculated based on the standard curve.

Monodansylcadaverine (MDC) staining

Autophagy Staining Assay Kit with MDC (Beyotime, C3018, Shanghai, China) was used to rapidly detect autophagy in HT22 cells. As described above, HT22 cells were treated. After the medium was removed, MDC staining solution was added and incubated for 1 h at 37 °C in the dark. When autophagy occurred, the green fluorescence was observed by fluorescence microscopy and analyzed by ImageJ.

RNA sequencing (RNA-seq)

To evaluate the changes in gene expression between control group, H_2O_2 group and hNSC-Exos group, total RNA was extracted from HT22 cells using standard extraction methods (Accurate Biology, AG21024, Beijing, China). After quality checks for purity, concentration, and integrity, oligo dT magnetic beads were specifically bound to the poly (A) tail of the mRNA to remove other RNAs, and the purified mRNA was fragmented. The treated mRNA was used as a template for reverse transcription to synthesize cDNA and for PCR amplification with primers. After purification, PCR was performed to establish a library. After quality inspection, the library was sequenced on a sequencer according to the manufacturer's operating guidelines. The R package was employed to analyze differences in mRNA expression levels between the two groups. DEGs with a P-value < 0.05 and FDR < 0.05 were considered statistically significant. The mRNA exhibiting differential expression was subsequently subjected to enrichment analysis based on Gene Set Enrichment Analysis (GSEA).

Double-label adenovirus mCherry-GFP-LC3B transfection and autophagy assay

HT22 cells were inoculated in confocal dishes (NEST, 726,001, Wuxi, China), and the experiment was conducted according to the transfection procedure for double-label adenovirus mCherry-GFP-LC3B (Beyotime, C3011, Shanghai, China). Upon infection with the Ad-mCherry-GFP-LC3B adenovirus, the mCherry-GFP-LC3B fusion protein is observed to emit a uniform yellow fluorescence across the cytoplasm under fluorescence microscopy in the absence of autophagy, resulting from the merged signals of mCherry and GFP. In contrast, during autophagic conditions, the protein localizes to the autophagosomal membranes, where it forms distinct yellow puncta. Following fusion of the autophagosomes with lysosomes, the fluorescence transitions to red puncta, a shift attributed to the selective quenching of GFP fluorescence. The number of yellow spots representing autophagic bodies and red spots representing autophagic lysosomes were counted.

Construction of HT22-KO-PINK1 Stable strain

HT22 cells were infected with PINK1-knockout lentivirus (Beyotime, L16306, Shanghai, China), and a stable KO-HT22 strain was constructed using Clustered Regularly Interspaced Short Palindromic Repeats -associated protein 9 (CRISPR/Cas9) technology. HT22 cells with good growth and 80% cell density were selected, spread on 6-well plates, and cultured in an incubator to determine the optimal multiplicity of lentivirus infection. The concentrated viral particles were added to the HT22 cell suspension. After 24 h of transfection, the medium containing the virus was discarded and replaced with a new medium for further culturing, and puromycin was added to screen for stable cell strains. Approximately 72 h after infection, different groups of KO-PINK1 were set up, and the expression of PINK1 in the protein was detected to evaluate the transfection efficiency, and the group with higher transfection efficiency was selected for subsequent experiments.

Animal model

According to the experiment requirement, male SD rats were divided into three groups, namely sham group,

MCAO group, and hNSC-Exos group (10 rats/group). All rats were anesthetized through intraperitoneal injection of 2.5% tribromoethanol (MedChemExpress, T48402, New Jersey, USA). They were fixed on the operating table in the supine position, and the neck skin was cut with surgical scissors to expose the carotid triangle. Similarly, the rats in the sham group were exposed only to the blood vessels, and the wounds were sutured immediately without further treatment. Rats in the MCAO and hNSC-Exos groups were further operated on. The right common carotid artery (CCA), external carotid artery (ECA), and internal carotid artery (ICA) were blunted separately to protect the vagus nerve. The proximal ends of the common and ECAs were ligated, and the ICA was clipped using an arterial clamp. An incision was made at the distal end of the CCA using ophthalmic scissors, and a thread plug (RWD, MSRC37B200PK50, Shenzhen, China, 250-280G, 5–6 mm) was slowly inserted into the ICA until it reached the bifurcation of the middle cerebral artery. After occlusion of the blood flow for 1.5 h, the thread plug was removed to restore blood flow for reperfusion was restored to successfully simulate CIRI [40]. Within 30 min after restoring blood flow, PBS (10 μL, sham group) or hNSC-Exos (7 μg/μL of hNSC-Exos dissolved in 10 μL of PBS, hNSC-Exos group) were delivered through an automatic brain stereo stereoscope (RWD, 71,001-S, Shenzhen, China), respectively, at the anterior (1.3 mm), lateral (3.5 mm), and ventral (6.5 mm) sites. The rats in the Sham group underwent the same operation of middle cerebral artery ischemia–reperfusion injury as the rats in the MCAO model group. It differs from the hNSC-Exos group, in which the Sham group was given PBS treatment to exclude the effect of the surgical procedure itself on the experimental results. We referred to the fourth edition of *the Rat Brain Stereotaxic Coordinates*. During the process, we adopted a double-blind test, that is, the subsequent examiners did not know the experimental rats in each group to minimize possible errors owing to subjective factors. Animals were excluded if they died prematurely. The legend shows the number of nude rats that provided data for analysis in each experiment.

Behavioral tests

The behavior tests were conducted by independent researchers who were unaware of the experimental group, and the data was analyzed by a separate researcher. The monitoring time points of neural function were referred to the published literature [41, 42].

Modified neurological severity score (mNSS)

The severity of nervous system damage in SD rats was evaluated. The mNSS scores were assessed before surgery, and 1, 2, 3, 5, 7 days after surgery, including motor (muscle strength status and abnormal movement), sensory (vision, touch, and proprioception), reaction, and balance tests. The total scores ranged from 0 to 18, with lower scores indicating more robust function, and higher scores indicating more severe impairment.

Cylinder experiment

Evaluation of motor sensory screening and detection of tactile responses and asymmetry in SD rats were conducted. Rats should familiarize themselves with the testing environment before the experiment. Before surgery, and 1, 3, 5, and 7 days postoperatively, each rat was placed in a transparent resin glass cylinder with a diameter of 20 cm and a height of 40 cm. The spontaneous standing exploration activity was observed for 5 min, and a video was recorded. The videos were analyzed to assess the preference of the left and right forelimbs of the rats for exploration. The asymmetry index was calculated as follows: percentage of the ipsilateral forelimb alone lying on the wall-percentage of the control forelimb alone lying on the wall. The greater the asymmetry index, the worse the motor coordination and the greater the motor cortex damage.

Adhesive tape removal experiment

Evaluation of motor sensory screening and detection of tactile responses and asymmetry in SD rats were performed. Before starting the experiment, the two front paws of the rats were pasted on the dorsal side of the rats' toes with a circular paper with a diameter of 8 mm (the animal was not covered, and were shaved before the experiment) for at least 3 days. The time for removing labels from both forelimbs of the rats will be recorded, and training will be conducted at least four times a day to select rats that can remove labels quickly from both forelimbs for inclusion. Before surgery, and 1, 3, 5, and 7 days postoperatively, a 5-mm diameter circular adhesive label was attached to the relatively hairless wrists of the rats to observe and record the time of label removal on the injured side.

Triphenyltetrazolium ammonium chloride (TTC) staining

All rats were randomly selected for TTC staining. After the rats were sacrificed (24 h later), the intact brain tissue was removed and placed in a refrigerator at −80 °C for 10 min. Subsequently, the brain tissue was cut into slices of approximately 2 mm thickness and incubated in 2, 3, 5-triphenyltetrazolium ammonium chloride (Solarbio, T8170, Beijing, China) for 30 min at 37 °C in the dark, with stirring to maintain uniform staining. After staining, a 4% paraformaldehyde (Biosharp, BL539A, Hefei, China) solution was fixed and photographed. Areas of

normal brain tissue appeared red, whereas infarcted areas appeared pale. ImageJ software was used to calculate the relative infarct volume of the brain tissue (percentage of cerebral infarct area/ total brain area).

Frozen section

It is prefered that the tissues to be examined using frozen sections be made of fresh material. The harvested rat brain tissues were fixed with 4% paraformaldehyde for 24 h. Subsequently, brain tissues were dehydrated using gradient concentrations of 10%, 20%, and 30% sucralose-PBS solutions. After dehydration, the brain tissue was soaked with opti-mum cutting temperature compound (Leica, 39,475,237, Heidelberg, Germany), followed by tissue fixation with a freezing microtome and serial slicing to a thickness of 20 μm.

Statistical analysis

All data were statistically analyzed using GraphPad Prism 9.0. The raw data of in vitro and in vivo experiments (such as protein expression levels, fluorescence intensity, etc.) were standardized using internal references. In addition, intention-to-treat analysis was used for statistical analysis of animal studies. For excluded experimental rats, we substituted their last available data to minimize the interpretation of the final findings due to animal exclusion. All experiments were repeated at least three times. Results are expressed as mean ± standard deviation. The student's t-test was utilized to analyze differences between two groups. For experiments with more than two groups, one-way analysis of variance (ANOVA) was applied, followed by Tukey's post hoc test and Student–Newman–Keuls (SNK)/ Least Significant Difference comparisons (LSD). $P \leq 0.05$ was considered statistically significant.

Results

Preparation and characterization of hNSC-Exos

hNSCs were meticulously isolated from the fetal forebrain tissues of healthy pregnant women who underwent elective termination of pregnancy. The cells were then cultivated in an adherent culture system within matrigel-coated flasks. As depicted in the flowchart, extracellular vesicles, designated as hNSC-Exos, were meticulously isolated from the culture supernatants of hNSCs through a series of differential gradient centrifugations (Fig. 1A). The adherently cultured hNSCs exhibited a characteristic fusiform or polygonal morphology under microscopic observation (Fig. 1B). Immunofluorescence staining with Nestin and SOX2, the archetypal markers of hNSCs, yielded robust positive signals, unequivocally confirming the neural stem phenotype of the cultured cells (Fig. 1C). The purified hNSC-Exos were rigorously characterized and authenticated using a trifecta of analytical techniques: WB, NTA, and TEM. WB analysis revealed the presence of hNSC-Exos surface markers, including CD9, CD63, CD81 and TSG101, with the absence of the negative marker Calnexin (Fig. 1D). The identification of marker proteins in exosomes generally involves the

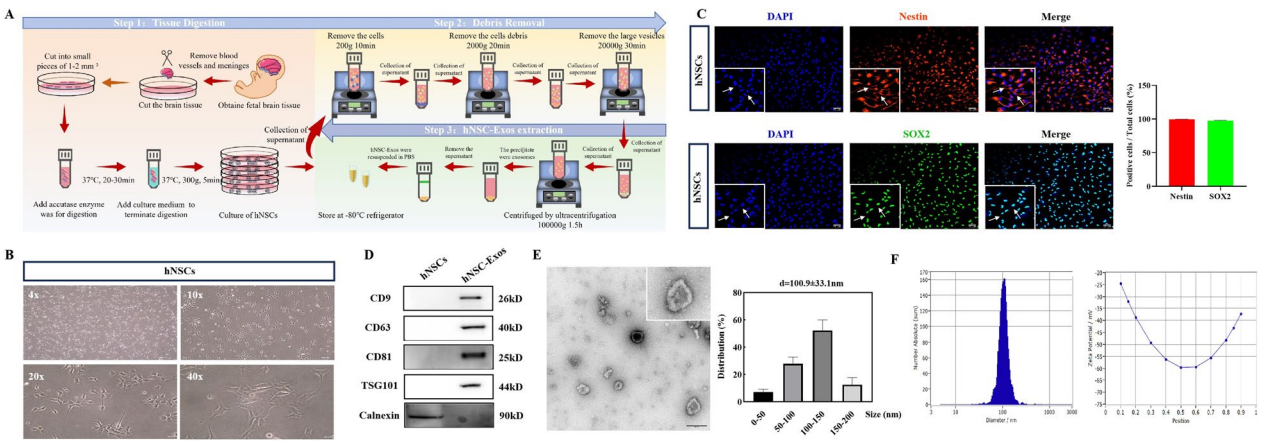

Fig. 1 Preparation and characterization of human neural stem cell-derived exosomes (hNSC-Exos). **A** The stepwise isolation process for hNSC-Exos, including ultracentrifugation and vesicle characterization. **B** The morphology of hNSCs were showed by light microscope (Imaging software: ViewPlayCap), scale bars: 200 μm, 100 μm, 50 μm, 20 μm. **C** Representative immunofluorescence visualization of hNSCs markers Nestin staining (red) and SOX2 staining (green) with DAPI-stained nuclei (blue) and the positive cells / total cells (%) was subsequently quantified by ImageJ, scale bar = 50 μm. The bottom left corner panel magnified the boxed area in the top panel. Data were presented as mean ± SD from three biological replicates, each performed in triplicate. **D** Western blotting (WB) analysis showed hNSC-Exos surface markers (CD9, CD63, CD81, and TSG101) and hNSCs cellular marker (Calnexin). Data from at least three biological replicates, each performed in triplicate. **E** The morphology of hNSC-Exos was observed by transmission electron microscopy (TEM) and the size distribution was quantified by ImageJ, scale bar = 200 nm. Data were presented as mean ± SD. **F** Nanoparticle tracking analysis (NTA) showed the size distribution and potential of hNSC-Exos

detection of at least three positive proteins and one negative protein. For positive protein markers, we selected the transmembrane proteins CD9, CD63, and CD81. As a negative protein marker, we chose the endoplasmic reticulum protein Calnexin. Most studies did not detect internal control proteins because the expression levels of actin, GAPDH, and Tubulin in exosomes are relatively lower compared to normal cell samples. TEM imaging depicted hNSC-Exos as possessing bilayer lipid membrane-bound structures with a distinctive "cup-mouth" morphology (Fig. 1E). The structure may be a form of exosome membrane when it reaches energy equilibrium, when the surface tension and internal pressure of the membrane reach a relatively stable state. NTA quantified the hNSC-Exos with diameters spanning 20 to 150 nm and zeta potentials ranging from −25 to −60 mV (Fig. 1F). The potential is negatively charged, which can reduce non-specific adsorption, and the absolute value of the potential is high, effectively indicating that the hNSC-Exos are uniformly dispersed and have high stability.

As suggested by Théry et al. [43], we adhered to the MISEV2018 guidelines for extracellular vesicle isolation and characterization. These findings corroborate the successful isolation of fully functional exosomes from the culture supernatant of hNSCs for subsequent experiments.

hNSC-Exos reversed the OS-induced neuronal injury in vitro

HT22 cells have the advantage of not expressing functional N-methyl-D-aspartic acid or α-Amino-3-hydroxy-5-methyl-4-isoxazolepropionic acid receptors and eliminating excitotoxic interference to focus on the direct effects of OS. Therefore, in this study, HT22 cells were employed and treated with H_2O_2 to construct an OS-induced injury model. To explore the potential of hNSC-Exos to reverse OS injury, we first ascertained whether hNSC-Exos could be effectively internalized by damaged neurons in vitro. We selected the commonly used lipophilic membrane dye PKH26 for labeling exosome internalization. At the same time, in order to minimize the impact of PKH26 dye specifically binding to other cellular components on the internalization results of exosomes, we performed multiple washes on the PKH26-labeled exosomes in vitro to remove any unbound or poorly bound excess dye. Afterward, PKH26-labeled hNSC-Exos were co-cultured with neurons, and the internalization process was visualized using fluorescence microscopy. Subsequently, hNSC-Exos labeled with PKH26 at different doses (1 μg, 5 μg, 10 μg, 20 μg, 40 μg) were co-cultured with neurons, and the internalization process was observed at 0 h, 2 h, 6 h, and 12 h using a fluorescence microscope. By calculating the positive cells in HT22 cells exposed to 400 μM H_2O_2, followed by treatment with different doses of PKH26 hNSC-Exos at different times (Fig. S1A), we found that the internalization of exosomes increased with time, most significantly at 6 h. Successful uptake was evidenced by the presence of PKH26-labeled hNSC-Exos within the cytoplasm of HT22 cells (Fig. 2A). At the same time, we supplemented flow assay to observe that CFDA SE-labeled hNSC-Exos was co-cultured at 0 h, 6 h to determine whether hNSC-Exos were internalized into the cells (Fig. S1B). The internalization was most obvious with the hNSC-Exos at doses of 20 μg and 40 μg. Therefore, for our subsequent in vitro experiments, we selected HT22 cells modeled with H_2O_2 for 6 h as H_2O_2 group, and the hNSC-Exos group was then administered with 20 μg exosomes. HT22 cells subjected to OS exhibited a decrease in cell count and displayed aberrant morphological characteristics, such as cellular shrinkage and deformation. Treatment with hNSC-Exos partially restored the cellular morphology (Fig. 2B), significantly enhanced the percentage of viable cells (Fig. 2C), and mitigated cytotoxicity (Fig. 2D). Given that H_2O_2-induced OS is a pathological mechanism implicated in neuronal apoptosis, Hoechst and TUNEL assays were employed to assess the protective effects of hNSC-Exos against H_2O_2-induced apoptosis in HT22 cells. Hoechst33258 staining revealed marked alterations in HT22 cells following H_2O_2 treatment, including condensed hyperchromatic nuclei and chromatin margination, indicative of early apoptosis. The nuclei appeared normal and blue following hNSC-Exos treatment (Fig. 2E). HT22 cells treated with H_2O_2 exhibited a higher apoptosis rate compared to the untreated group, which was significantly reduced after hNSC-Exos treatment (Fig. 2F), suggesting that hNSC-Exos afforded protection to the H_2O_2-induced OS model of HT22. Subsequently, we evaluated cell apoptosis utilizing annexin V-FITC/PI double staining in conjunction with flow cytometry and observed that hNSC-Exos markedly diminished the level of H_2O_2-induced early apoptosis (Annexin V^+/PI^-, 12.52–2.02%), rather than late apoptosis (Annexin V^+/PI^+, 0.9–0.41%) (Fig. 2G). Therefore, we speculate that hNSC-Exos mainly inhibits early apoptosis. qRT-PCR data indicated that the levels of the pro-apoptotic marker Bax were reduced, whereas those of the anti-apoptotic marker BCL2 were elevated following hNSC-Exos treatment (Fig. 2H). Furthermore, in the early stage of apoptosis, Cleaved caspase 3 is activated and accumulated, indicating that the cells are undergoing programmed death through the classical mitochondrial-dependent apoptosis pathway. WB analysis showed that hNSC-Exos increased the level of Caspase 3 and reduced the level of Cleaved caspase 3 (Fig. 2I), suggesting that hNSC-Exos may have anti-apoptotic or neuroprotective

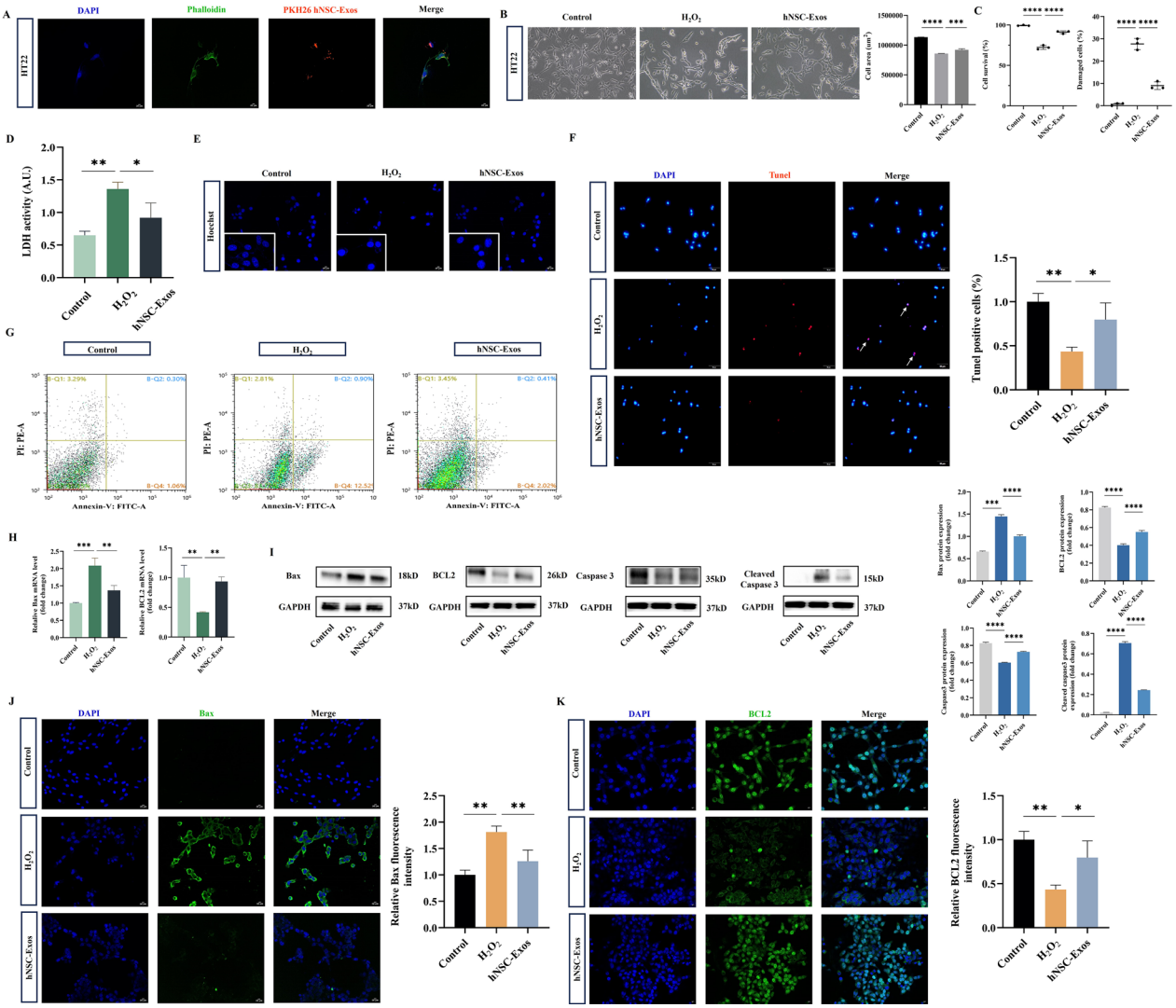

Fig. 2 hNSC-Exos reversed OS-induced neuronal injury in vitro. **A** Representative immunofluorescence of PKH26-stained hNSC-Exos (red) into the cytoskeleton (green) labeled with phalloidin and DAPI-stained nuclei (blue), scale bar = 20 μm. **B** HT22 cell morphology under a light microscope and the cell areas were quantified by ImageJ, scale bar = 20 μm. **C** Cell survival and damag rate, as indicated by trypan blue counting. **D** LDH was used to detect cell toxicity. **E** Hoechst33258 staining was used to observe the nuclear morphology (blue) of HT22, scale bar = 20 μm. The bottom left corner panel magnifies the boxed area in the top panel. **F** TdT-mediated dUTP nick end labeling (TUNEL) staining (red) was used to detect apoptosis, cell nuclei were counterstained with DAPI (blue), scale bar = 50 μm. The proportion of apoptotic cells was quantified by ImageJ. **G** Flow cytometry analysis of cell apoptosis. The loop gate was set according to the cell population position of the control group, which was divided into 4 quadrants. Annexin V^+/PI^- for early apoptosis and Annexin V^+/PI^+ for late apoptosis. **H** mRNA levels of Bax and BCL2 were measured using qRT-PCR, and data were normalized to actin mRNA expression. **I** WB was used to analyze apoptosis markers, hNSC-Exos significantly reduced Bax and Caspase3 expression, increased BCL2 and Cleaved caspase 3 expression compared to H_2O_2-treated cells. The data were normalized to GAPDH protein expression. (**J** and **K**) Representative immunofluorescence staining image of Bax staining (green) and BCL2 staining (green) with DAPI-stained nuclei (blue), and the relative Bax and BCL2 fluorescences were quantified by ImageJ, scale bar = 20 μm. *P < 0.05, **P < 0.01, ***P < 0.001, ****P < 0.0001. Data were presented as mean ± SD from three biological replicates, each performed in triplicate. The "Control" group represents untreated HT22 cells, the "H_2O_2" group comprises HT22 cells exposed to 400 μM H_2O_2, and the "hNSC-Exos" group consists of HT22 cells exposed to 400 μM H_2O_2, followed by treatment with 20 μg hNSC-Exos

effects. Additionally, immunofluorescence for Bax and BCL2 further corroborated that hNSC-Exos exerted a protective effect against H_2O_2-induced apoptosis in HT22 cells (Fig. 2J-K). These findings collectively suggest that hNSC-Exos have the capacity to reverse neuronal apoptosis in vitro. Moreover, as the background of this study is based on the secondary damage of CIRI, we have demonstrated through multidimensional synergy that

hNSC-Exos mainly repair damaged neurons by affecting early stage of apoptosis.

hNSC-Exos alleviated neuronal injury after ischemic stroke

In our study, we confirmed that hNSC-Exos have the ability to reverse OS-induced neuronal injury in vitro. Building upon this finding, we then explored the impact of hNSC-Exos on brain injury in rats subjected to MCAO. Reperfusion was initiated 1.5 h after MCAO was established (Fig. 3A). The hNSC-Exos treatment group received the therapeutic intervention concurrently, and all assessments were conducted at the designated time points. To ascertain whether hNSC-Exos could repair neuronal apoptotic damage in the brains of MCAO rats, we investigated whether PKH26-labeled hNSC-Exos could be effectively internalized by neurons in the brain in vivo. We observed that hNSC-Exos accumulated at the site of brain injury and were taken up by neurons 24 h post-injection (Fig. 3B). We have taken various measures to evaluate the neuroprotective effects of hNSC-Exos on MCAO. First, brain tissues were harvested for TTC staining one day after hNSC-Exos transplantation to compare the volume of cerebral infarction in each group of rats (Fig. 3C). The brain tissue of the sham group appeared normal in gross anatomy, with no visible infarct lesions. The right hemisphere of the MCAO group showed pallor and absence of vascular distribution, and the coronal brain tissue sections revealed a large area of white infarct in the right side. The volume of cerebral infarction in the hNSC-Exos group was significantly smaller than that in the MCAO group. Next, we evaluated the neurological deficits and recovery of the experimental rats, including mNSS to assess motor, sensory, and reflex functions. The cylinder experiment to evaluate the degree of forepaw asymmetry and the adhesive removal experimentexperiment to determine skin sensitivity and the integrity of sensory function. These are common behavioral methods for assessing CNS diseases. Generally, assessments within 7 days of MCAO can better reflect the neurological function during the acute phase, and animals will experience a certain degree of self-recovery after 7 days [42]. Considering that this study focuses on the changes in neurons during CIRI, we conducted behavioral assessments as a baseline for the MCAO and hNSC-Exos groups before surgery, and evaluated them on days 1, 3, 5, and 7 after surgery, respectively. The results suggested that both groups exhibited neurological deficits with no significant differences after modeling. Behavioral changes in each group of rats were recorded on baseline, days 1, 3, 5, and 7 after hNSC-Exos transplantation. Compared to the MCAO group, the hNSC-Exos treatment group demonstrated a significant reduction in neurological deficits following MCAO (Fig. 3D), the frequency of the cylinder hitting the wall (Fig. 3E), and the time required to remove the sticky patch in the stick-and-stick experiment (Fig. 3F). The results suggested that hNSC-Exos offer neuroprotective benefits. TUNEL fluorescence staining was conducted (Fig. 3G). Minimal apoptotic cells were detected in the sham group, whereas a significant number of apoptosis-positive cells were observed in the MCAO group. The number of apoptosis-positive cells in the brain neurons of MCAO rats was markedly reduced 24 h after hNSC-Exos treatment. We further analyzed the expression of several apoptotic markers using WB and found that hNSC-Exos diminished the expression of Bax and Cleaved caspase 3, while increasing the levels of BCL2 and Caspase 3 (Fig. 3H). These findings lend support to the hypothesis that hNSC-Exos can alleviate brain injury subsequent to MCAO.

hNSC-Exos rescued mitochondrial dysfunction by promoting mitophagy

As the repairing effect of hNSC-Exos on OS-induced neuronal apoptosis has been preliminarily confirmed in vitro and in vivo, we further investigate its main mechanism. We know that neurons heavily depend on

(See figure on next page.)

Fig. 3 hNSC-Exos alleviated neuronal injury after middle cerebral artery occlusion rats (MCAO). **A** Schematic diagram of the in vivo experiment: reperfusion was given 1.5 h after establishing MCAO, and the hNSC-Exos was given simultaneously, and the tests were performed at the corresponding time points. **B** Fluorescence staining was used to observe the uptake of PKH26-labed hNSC-Exos by neurons in the brain at 24 h after injection. The bottom left corner panel magnifies the boxed area in the top panel. The percentage of PKH26 positive cells was quantified by ImageJ. **C** Triphenyltetrazolium ammonium chloride (TTC) staining was used to determine cerebral infarct volume (white area, n = 3 rats/group), scale bar = 3 mm. The neurological function score (**D**), cylinder test (**E**), and stick test (**F**) were used to evaluate the neuroprotective effect of hNSC-Exos on MCAO rats before surgery (baseline) and day 1, 2, 3, 5, and 7 after surgery, n = 8 rats/group. The neurological function score ranged from 0 to 18 and the asymmetry index was calculated as percentage of the ipsilateral forelimb alone lying on the wall—percentage of the control forelimb alone lying on the wall. **G** TUNEL staining (red) was used to detect the apoptosis in brain neurons (green) in MCAO rats, and DAPI staining (blue) was used to stain the nucleus (n = 6 rats/group), scale bar = 20 μm. **H** WB analysis of the expression of apoptosis-related indicators Bax, BCL2, Caspase 3, and Cleaved caspase 3, and the data were normalized to GAPDH protein expression (n = 6 rats/group). *P < 0.05, **P < 0.01, ***P < 0.001, ****P < 0.0001. Data were presented as mean ± SD from three biological replicates, each performed in triplicate. The "Sham" group represents sham surgery rats, the "MCAO" group represents middle cerebral artery occlusion rats, and the "hNSC-Exos" group represents MCAO rats treated with 70 μg hNSC-Exos

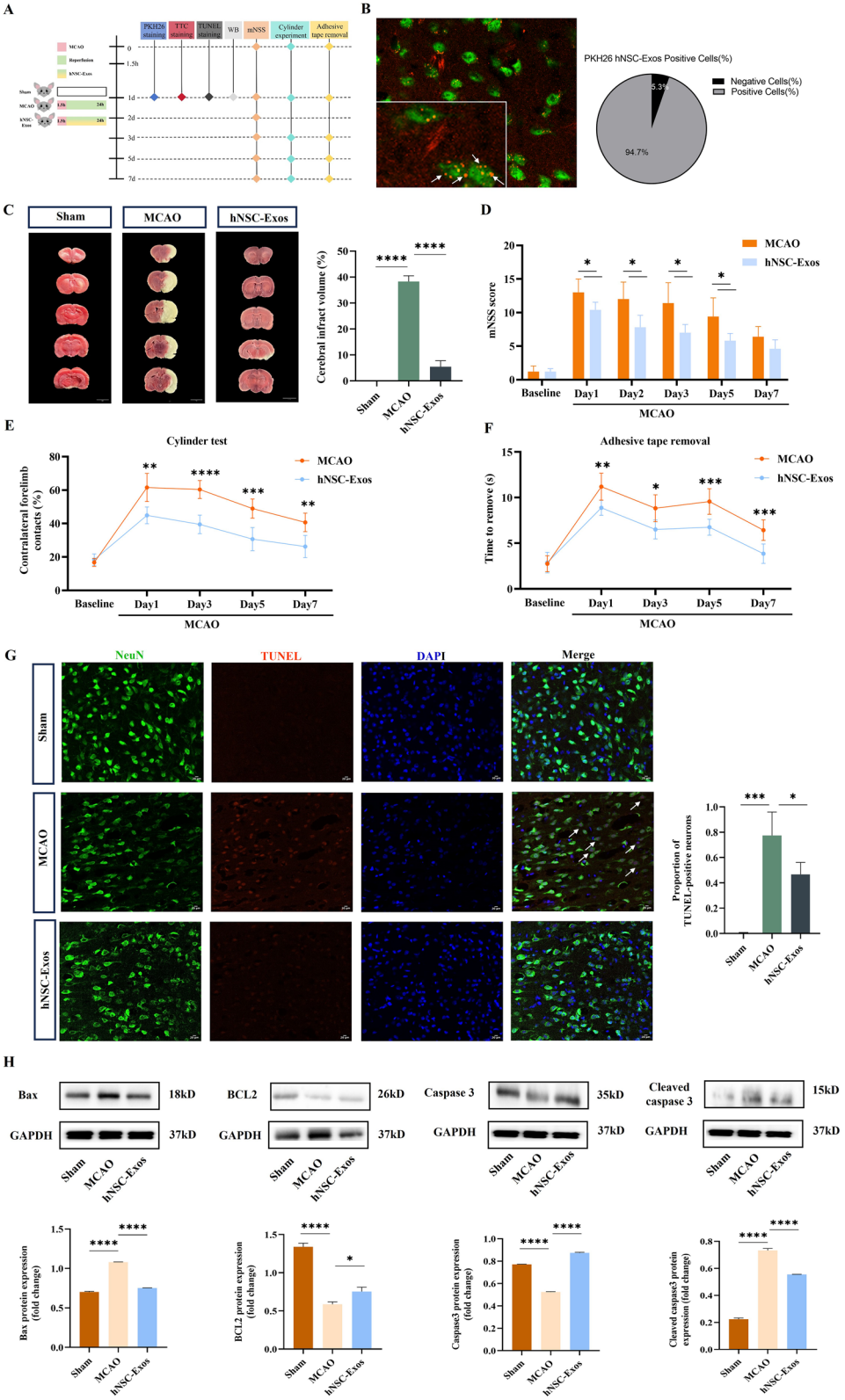

Fig. 3 (See legend on previous page.)

mitochondria to meet the energy demands of synaptic transmission. After CIRI, mitochondrial dysfunction can occur, the mitochondrial membrane potential decreased, the red fluorescence of mitochondria was gradually weakened, and the green fluorescence appeared positive (Fig. 4A). In addition, compared with the H_2O_2 group, lower total cellular ROS levels (Fig. 4B) and lipid peroxidation (Fig. S2) were detected in the hNSC-Exos group, confirming the antioxidant capacity of hNSC-Exos. In order to deeply analyze the mechanisms of gene expression regulation, transcriptomic analysis was performed on HT22 cells with or without H_2O_2 induction treatment. There was a significant difference in the transcriptome between the H_2O_2 group and the control group, and gene set enrichment analysis showed that lysosomal genes were upregulated in the H_2O_2-induced damaged neuron group (Fig. 4C). An increase in lysosomal abundance may enhance the susceptibility of damaged mitochondria to recognition and degradation by the autophagic machinery. Furthermore, the acidic milieu within lysosomes can avert the retardation of degradation that might result from inadequate acidification following the conjugation of autophagosomes with lysosomes. We compared the expression of lysosomal genes in the control group and the H_2O_2 group by qRT-PCR based on the statistically significant changes in lysosomal genes in the sequencing data (Fig. S3). The results, consistent with the sequencing data, further verified that the lysosomal genes in OS-induced neurons were upregulated. Therefore, in light of the critical role of autophagy in neuronal apoptosis, we propose the hypothesis that autophagy may occur in H_2O_2-induced HT22 cells. First, the green fluorescent bright spots on MDC staining were characteristic of changes in autophagy (Fig. 4D). Subsequently, in order to investigate whether hNSC-Exos reduce neuronal damage by regulating the autophagy pathway, we combined multidimensional detection of autophagy occurrence, including transfection of HT22 cells with Ad-mCherry-GFP-LC3B fusion gene adenovirus to observe fluorescence intensity, TEM to observe mitochondrial morphology, WB and immunofluorescence staining were used to detect the expression of mitophagy related indicators. The results suggest that yellow spots (combined by mCherry and GFP fluorescence) indicate autophagosomes that are not fused to lysosomes, whereas red spots (mCherry fluorescence) indicate autophagosomes fused to lysosomes. It can be seen that the increase of red and yellow dots indicates that autophagy is activated, suggesting that hNSC-Exos can induce autophagy in neurons (Fig. 4E). Similarly, TEM showed mitochondrial membrane damage, swelling, fewer mitochondrial cristae, vacuolization, and a few autophagosomes after H_2O_2 induction (Fig. 4F). The numbers of autophagosome per filed were quantified by ImageJ. Whereas mitochondrial damage was recovered, and autophagosomes were increased after hNSC-Exos treatment. We know that mitophagy begins with the formation of phagosomes. Beclin is significant in initiating autophagy, and LC3B is an autophagy marker. This result was demonstrated by WB in vivo (Fig. 4G) and in vitro (Fig. 4H) experiments, indicating that hNSC-Exos enhanced the expression levels of mitophagy-related proteins (PINK1, Parkin, Beclin, and LC3B). The results of the WB analysis were confirmed by immunofluorescence analysis that PINK1 (Fig. 4I), Beclin (Fig. 4G), and LC3B (Fig. 4K) expression levels were increased in OS, and the levels of these mitophagy-related proteins were further increased after hNSC-Exos treatment. At the same time, we compared

(See figure on next page.)

Fig. 4 hNSC-Exos rescued mitochondrial dysfunction by promoting mitophagy. **A** Mito Tracker Red CMXRos, a red fluorescent probe dependent on mitochondrial membrane potential, and Annexin V-FITC, a green fluorescent probe for cell apoptosis, were used to jointly detect mitochondrial membrane potential level (red) and apoptosis (green), scale bar = 20 μm. The ratio of red/green fluorescence was quantified by ImageJ. **B** Representative fluorescence image and quantification of reactive oxygen species (ROS) (green), scale scale = 50 μm. The mean ROS fluorescence was quantified by ImageJ. **C** RNA-seq analysis revealed increased lysosomal gene expression in OS-treated neurons, suggesting a role for lysosomes in mitophagy activation ('NC1' refers to the 'Control' group, 'NC2' refers to the 'H_2O_2' group)". **D** Monodansylcadavrine (MDC) autophagy fluorescent staining (green), scale bar = 20 μm. The percentage of proportion of MDC-positive cells was quantified by ImageJ. **E** Representative image of HT22 cells transfected with Ad-mCherry-GFP-LC3B adenovirus. Autophagosomes are labeled by red and green fluorescence (yellow dots), whereas autophagic lysosomes are labeled by red fluorescence (red dots). The expression of red and yellow dots was observed in each cell. The bottom left corner panel magnifies the boxed area in the top panel, scale bar = 50 μm. The percentage of autophagosomes & autolysosomes per cell was quantified by ImageJ. **F** Mitochondrial morphology and the number of autophagosomes were observed and quantified through TEM, red arrow indicates mitochondria, and circle indicates autophagosomes, scale bar = 500 nm. The numbers of autophagosome per filed were quantified by ImageJ. WB analysis showed the expression of mitophagy-related proteins (PINK1, Parkin, Beclin, and LC3B) in vitro (**G**) and in vivo (**H**). hNSC-Exos significantly increased mitophagy-related proteins expression compared to H_2O_2-treated cells. Data were normalized to GAPDH protein expression (n = 6 rats/group). Representative images of (**I**) PINK1, (**J**) Beclin staining (green) and (**K**) LC3B staining (red) with DAPI-stained nuclei (blue), scale bar = 20 μm. *P < 0.05, **P < 0.01, ***P < 0.001, ****P < 0.0001. Data were presented as mean ± SD from three biological replicates, each performed in triplicate. Experimental groups ('Control,' 'H_2O_2,' and 'hNSC-Exos') were as described in Fig. 2. Experimental groups ('Sham,' 'MCAO,' and 'hNSC-Exos') were as described in Fig. 3

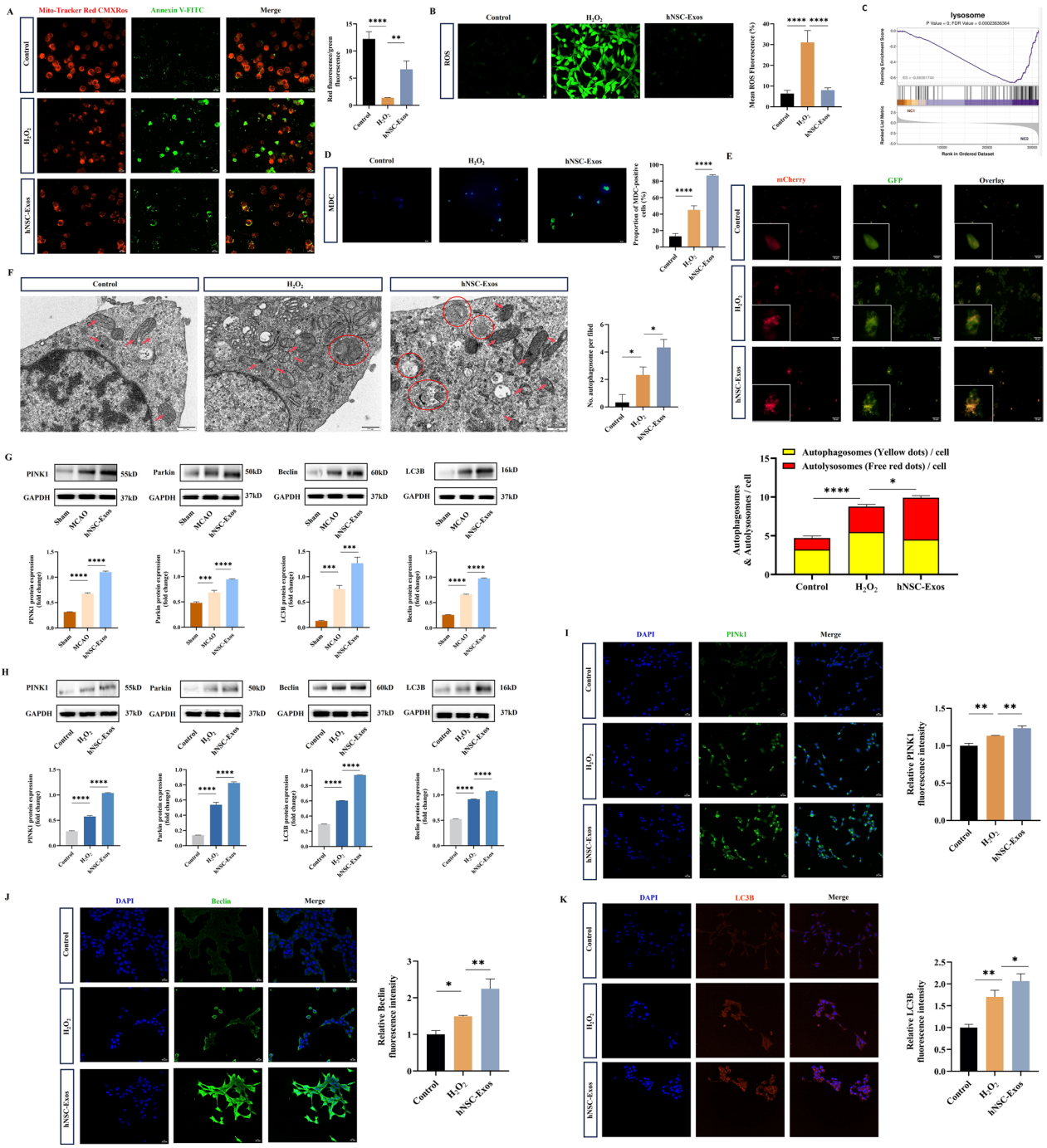

Fig. 4 (See legend on previous page.)

the transcriptomic results of hNSC-Exos group and H_2O_2 group on the regulation of neuron function, and found that hNSC-Exos up-regulated the expression of synaptic adhesion protein, which can drive the formation of synapses in neurons (Fig. S4). These results demonstrate that hNSC-Exos rescued mitochondrial dysfunction by promoting mitophagy in vitro and in vivo.

hNSC-Exos promoted mitophagy by activating the PINK/Parkin pathway

As mentioned earlier, mitophagy is a selective autophagy that maintains the integrity of mitochondrial function and cellular homeostasis by specifically clearing dysfunctional mitochondria in the cytoplasm. PINK1/Parkin is one of the most important mitophagy pathways.

To elucidate the primary role of mitophagy in the reversal of OS-induced neuronal injury by hNSC-Exos, we conducted experiments that revealed a decrease in the expression of key mitophagy-related proteins (PINK1, Parkin, Beclin, and LC3B) following the administration of the mitophagy inhibitor mdivi-1. Notably, treatment with hNSC-Exos significantly restored mitophagy (Fig. 5A). The application of mdivi-1 also led to a reduction in ROS production (Fig. 5B) and mitochondrial membrane potential (Fig. 5C), partially negating the reparative effects of hNSC-Exos on mitochondria. While mitophagy is not a solitary signaling cascade, it is intricately linked with apoptosis. It facilitates the swift degradation of impaired mitochondria, thereby inhibiting apoptosis. Upon inhibition of mitophagy, there was an upregulation of pro-apoptotic markers such as Bax and Cleaved caspase 3, and a corresponding downregulation of anti-apoptotic markers including BCL2 and Caspase 3. In contrast, hNSC-Exos treatment significantly mitigated pro-apoptotic markers and enhanced anti-apoptotic markers (Fig. 5D). These findings offer compelling evidence that hNSC-Exos trigger mitophagy in neurons that have been compromised by OS.

Our findings underscore the pivotal role of hNSC-Exos in countering intracellular OS through the autophagy-lysosomal cascade and in modulating the PINK1/Parkin mitophagy pathway to mitigate neuronal apoptosis and facilitate neuronal regeneration. To corroborate the significance of the PINK1/Parkin signaling axis in counteracting OS-induced neuronal injury, we employed PINK1-knockout lentivirus to manipulate HT22 cells, thus assessing the mitophagy-related impacts for validation. Following the PINK1 protein expression profiling, the KO-PINK1 cells treated with the secondary co-staining reagent were meticulously analyzed (Fig. 6A). In alignment with prior studies, the expression levels of mitophagy-related proteins (PINK1, Parkin, Beclin, and LC3B) were observed to decline post-PINK1 knockout, and the augmenting influence of hNSC-Exos on mitophagy was diminished (Fig. 6B). Furthermore, the reduction in red and yellow spots upon PINK1 depletion signified a decrease in autophagy levels, whereas hNSC-Exos exerted a certain degree of upregulation on these spots (Fig. 6C). We delved deeper to discern whether the PINK1/Parkin mitophagy triggered by hNSC-Exos could ameliorate the mitochondrial dysfunction induced by H_2O_2. The mitophagy-promoting effects of hNSC-Exos were substantially impeded by the absence of PINK1 (Fig. 6D). Moreover, the KO-PINK1 + hNSC-Exos group exhibited reduced mitochondrial ROS levels compared to the KO-PINK1 group, affirming the antioxidant potential of hNSC-Exos via the PINK1 pathway (Fig. 6E). Similarly, the impact of hNSC-Exos on pro- and anti-apoptotic markers was somewhat constrained in the absence of PINK1 (Fig. 6F). Collectively, our data indicate that hNSC-Exos enhance mitophagy by stimulating the PINK1/Parkin pathway, thereby attenuating mitochondria-dependent apoptosis.

Discussion

To our knowledge, this study has identified a novel therapeutic approach using hNSC-Exos to target mitochondria, demonstrating their ability to modulate the PINK1/Parkin mitophagy pathway and reduce OS-induced neuronal apoptosis. OS damage has been mechanistically linked to both the occurrence and progression of CIRI-induced neuronal dageneration [44], while emerging evidence underscores the therapeutic potential of hNSC-Exos in mediating neuroprotective effects and promoting neural repair in various neurological pathologies [12, 45, 46]. Therefore, we have demonstrated in vitro and in vivo that hNSC-Exos can alleviate OS-mediated neuronal damage during CIRI. RNA-Seq revealed a notable upregulation of lysosome content under OS conditions. As a highly conserved organelle in eukaryotic cells, lysosomes function as central regulatory nodes integrating multiple cellular signaling cascades, with demonstrated critical involvement in both metabolic homeostasis and immunological surveillance [47, 48]. Damaged mitochondria are specifically encapsulated into autophagosomes and fused with lysosomes, completing the degradation of mitochondria and maintaining the stability of the intracellular environment, a process known as mitophagy [49]. However, whether hNSC-Exos are involved in the

(See figure on next page.)

Fig. 5 hNSC-Exos enhanced mitophagy in damaged neurons. **A** WB analysis showed the expression of mitophagy-related proteins (PINK1, Parkin, Beclin, and LC3B), and data were normalized to GAPDH protein expression. **B** Representative fluorescence image of ROS (green), scale bar = 50 μm. The mean ROS fluorescence was quantified by ImageJ. **C** Mito Tracker Red CMXRos and Annexin V-FITC were used to jointly detect mitochondrial membrane potential level (red) and apoptosis (green), scale bar = 20 μm. The ratio of red/green fluorescence was quantified by ImageJ. **D** The expression of apoptosis-related indicators Bax, BCL2, Caspase 3, and Cleaved caspase 3, and data were normalized to GAPDH protein expression. *P < 0.05, **P < 0.01, ***P < 0.001, ****P < 0.001, ****P < 0.0001. Data were presented as mean ± SD from three biological replicates, each performed in triplicate. Experimental groups ('Control', 'H_2O_2,' and 'hNSC-Exos') are as described in Fig. 2. The "Mdivi-1" group comprises HT22 cells exposed to 400 μM H_2O_2 while also being treated with the mitophagy inhibitor 10 μM Mdivi-1, and the "Mdivi-1 + hNSC-Exos" group consists of HT22 cells exposed to 400 μM H_2O_2 while also being treated with the mitophagy inhibitor 10 μM Mdivi-1, followed by treatment with hNSC-Exos

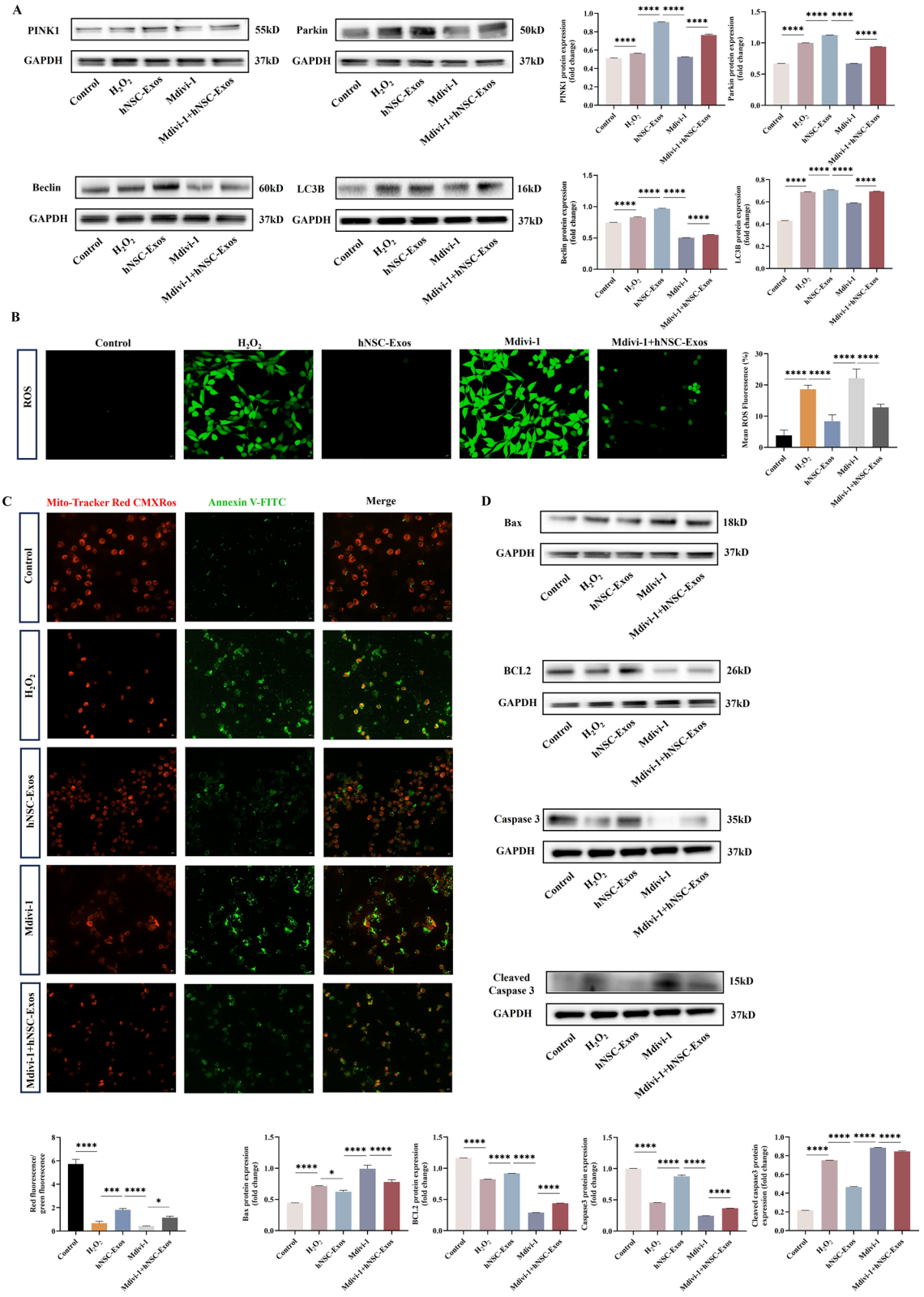

Fig. 5 (See legend on previous page.)

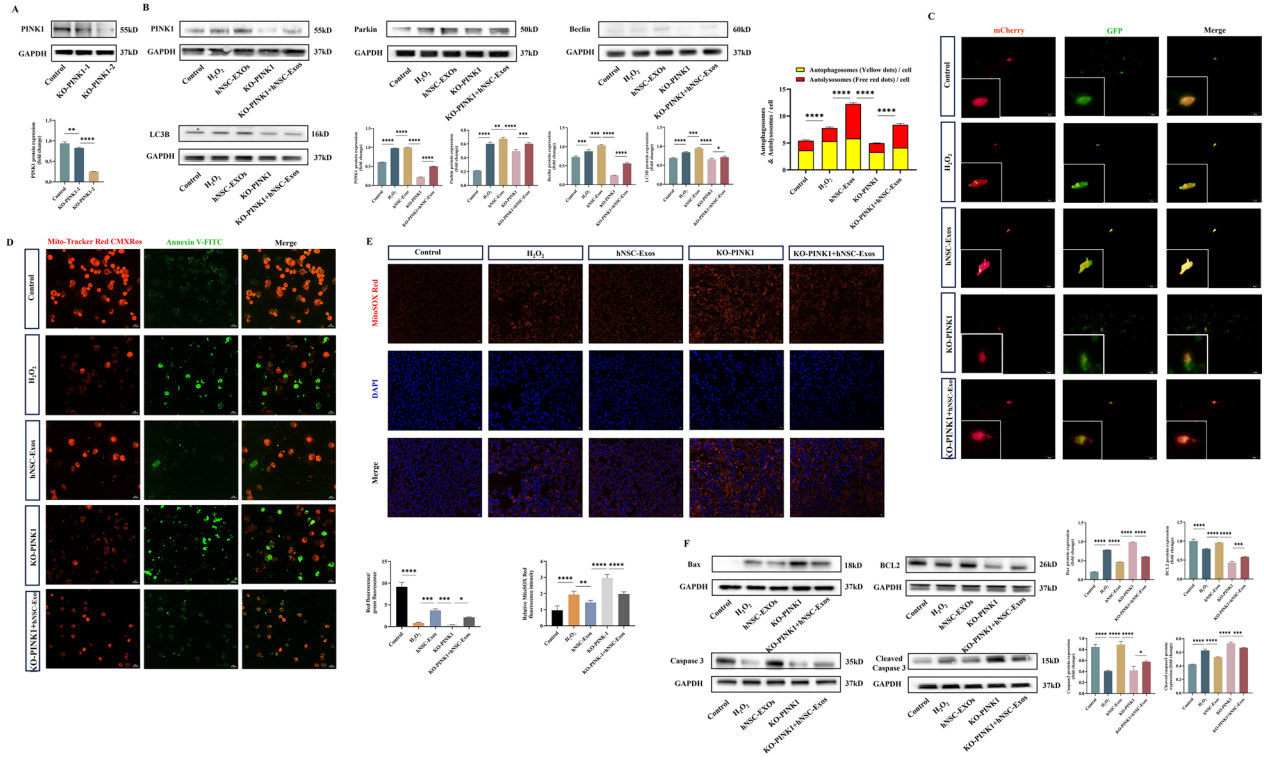

Fig. 6 hNSC-Exos enhanced mitophagy by activating the PINK1/Parkin pathway. **A** HT22 was infected with PINK1 gene knockout lentivirus, and then the expression of PINK1 protein in transfection groups was detected by WB analysis. The group with relatively obvious expression was selected to simulate the KO-PINK1 model for experiments. **B** WB analysis showed the expression of mitophagy-related proteins (PINK1, Parkin, Beclin, and LC3B), and the data were normalized to GAPDH protein expression. **C** The expression of fluorescence (red dots) and autophagosomes (yellow dots) were observed. The bottom left corner panel magnifies the boxed area in the top panel, scale bar = 50 μm. The percentage of autophagosomes& autolysosomes per cell was quantified by ImageJ. **D** Mito Tracker Red CMXRos and Annexin V-FITC were used to jointly detect mitochondrial membrane potential level (red) and apoptosis (green), scale bar = 20 μm. The ratio of red/green fluorescence was quantified by ImageJ. **E** Representative fluorescence image of MitoSOX (red) and the mean mitoSOX red fluorescence was quantified by ImageJ, scale bar = 20 μm. **F** Expression of apoptosis-related markers Bax, BCL2, Caspase 3, and Cleaved caspase 3, and data were normalized to GAPDH protein expression. *P < 0.05, **P < 0.01, ***P < 0.001, ****P < 0.0001. Data were presented as mean ± SD from three biological replicates, each performed in triplicate. Experimental groups ('Control,' 'H_2O_2,' and 'hNSC-Exos') are as described in Fig. 2. The "KO-PINK1" group comprised HT22 cells in which the PINK1 gene had been knocked out and were then exposed to 400 μM H_2O_2, and the "KO-PINK1 + hNSC-Exos" group consists of HT22 cells in which the PINK1 gene had been knocked out and were then exposed to 400 μM H_2O_2, followed by treatment with hNSC-Exos

occurrence of mitophagy and how this process mediates the recovery of neuronal function requires further exploration. The results show that hNSC-Exos exert their therapeutic effects through precise modulation of the PINK1-Parkin mitophagy pathway, concurrently demonstrating therapeutic efficacy in behavioral improvement in MCAO rats. In our study, the use of exosomes provides a safer and more efficient alternative to NSC delivery. These results represent significant advancements and therapeutic mechanisms in the treatment of IS with hNSC-Exos.

CIRI constitutes a multifactorial pathophysiological cascade encompassing diverse molecular pathways. The pathogenesis of IS has been extensively investigated through both basic science and clinical studies over decades. Although blood flow restoration through reperfusion is therapeutically essential, this process results in irreversible cerebral damage, neuronal degeneration, and even cell death, involving many complex pathological cascades including OS, inflammatory response, and calcium overload. During CIRI progression, superoxide anion free radicals, hydroxyl radicals, and nitric oxide are produced, and the excessive ROS-establishes a oxidative microenvironment that triggers neuronal apoptosis [50]. Our investigation systematically elucidated the direct detrimental effects of OS on mitochondrial structure and bioenergetics in neurons. Utilizing an in vitro H_2O_2-induced OS model, we observed significant structural disintegration (manifested by cristae disruption) and functional impairment of mitochondria: diminished

mitochondrial membrane potential (an early apoptotic indicator), elevated ROS levels (reflecting antioxidant system collapse). These results consistent with published findings [16, 51, 52]. Therefore, effectively eliminating the oxidative microenvironment during CIRI is essential for rescuing damaged neurons. Current clinical management relies on two pharmacological agents—edaravone [53] and butylphthalide [54]—which demonstrate partial efficacy in OS attenuation but face therapeutic limitations including poor target specificity, suboptimal bioavailability, restricted multi-target engagement capacity, and rapid metabolic clearance. Within this therapeutic context, our study provides insights into mitochondrial protective mechanisms, potentially informing the development of novel targeted therapeutic strategies for IS.

We have developed a novel mitochondria-targeting therapeutic strategy utilizing hNSC-Exos [17, 55, 56], which target damaged areas and deliver tissue-specific neurogenic differentiation inducers and neurotrophic factors. This is critical for scavenging ROS to protect damaged neurons and reduce secondary injury following CIRI. Edaravone is currently the most widely used free radical scavenger in clinical practice [37], which inhibits the peroxidation of brain cells by breaking the lipid peroxidation reaction chain, thereby protecting neurons and delaying neuronal apoptosis. Other excitatory amino acid antagonists, calcium channel blockers, and endogenous free radical scavengers also have therapeutic effects on CIRI injury, but it is difficult to achieve efficacy through monotherapy [57]. The unique physicochemical properties and biological potency of hNSC-Exos confer distinct therapeutic advantages. Compared to those traditional drugs, which can only partially penetrate the BBB, hNSC-Exos can efficiently cross the BBB through mechanisms such as phagocytic transport and membrane fusion. Moreover, it actively targets the ischemic injury area through receptor ligand interaction by relying on the surface facial mask protein to achieve higher efficacy. This provides theoretical support for its efficient treatment. Furthermore, the safety of hNSC-Exos has been significantly enhanced. Due to the effective dose being low, the risk of embolism is significantly reduced, and the lack of MHC-II molecules on their surface avoids triggering a systemic immune response. Therefore, our research team has been developing and utilizing hNSCs and their secretions to treat CNS diseases based on OS, and collaborating with international peers to focus on treating major neurological diseases [58]. We successfully isolated hNSCs from the forebrain tissue of aborted fetuses, which were collected from healthy pregnant women requesting abortion, and extracted hNSC-Exos from hNSCs [38]. In this study, we conducted both in vitro and in vivo experiments to validate our hypothesis that hNSC-Exos are essential for promoting the health of damaged neural cells. In our previous study [39], by comparing the uptake efficiency of hNSC-derived vesicles by different cell types in brain-like organs, we found that neurons have a slightly higher uptake efficiency than neural progenitor cells (NPCs) and glial progenitor cells (GPCs). This provides a certain preliminary basis for choosing neurons as the OS-model in this study. When PKH26-labeled hNSC-Exos were added to the experiments, consistent with previous studies, we found that they homed to the damaged neuronal areas in the OS environment. In this process, we observed an interesting phenomenon where the diameter of fluorescence-stained hNSC-Exos was much larger than that detected by NTA, suggesting that the possible mechanism for this size increase is the aggregation/fusion of PKH nanoparticles with exosomes or the insertion of PKH molecules into the exosome membrane. Studies have shown that even when PKH is diluted to the point where fluorescence is reduced to the detection limit (0.16 μM), making it difficult to detect fluorescence signals at this concentration, the increase in particle size of exosome caused by PKH can still be observed [59]. This demonstrates that exosomes are successfully taken up by damaged neurons and produce a therapeutic effect.

In this study, we used an ischemia–reperfusion rat model to simulate CIRI and observed the histological and behavioral changes in MCAO rats during hNSC-Exos treatment, including neuronal apoptosis and impaired neurological function. Neurons, as the fundamental functional units of the brain, are widely considered to be a key factor in the apoptotic damage of brain tissue. To our knowledge, there is no consensus on the dose of hNSC-Exos used in animal model treatments, and the selection of dosage is primarily based on experience. However, by reviewing the published literature, we found that stereotactic administration is a frequently chosen method compared to traditional arteriovenous injection, as it can deliver hNSC-Exos more directly to the damaged area, thereby enhancing the therapeutic effect [60]. The usual administration time is within 24 h after ischemia, with a dosage range of 10–100 μg per rat. Based on the experimental purpose of exploring the mechanism of CIRI damage and preliminary research results [39, 61], we determined that using 70 μg of hNSC-Exos per rat was safe and effective. TTC results suggested that hNSC-Exos significantly reduced the volume of cerebral infarction. Next, to assess the degree of neurological damage in the rats, we used TUNEL staining and a variety of behavioral assessment methods, including mNSS scoring, the rotarod test, and the adhesive tape removal test. The results showed that hNSC-Exos significantly reduced the apoptosis of damaged neurons in the rats. Although on

the 7th day after treatment, there was no statistical difference in mNSS scores between the MCAO group and the hNSC-Exos treatment group. This may be due to small sample sizes or variability in spontaneous recovery of the MCAO group rats. In addition, the reduction of the Bax index and the upregulation of the BCL2 index in the brain tissue of MCAO rats by hNSC-Exos further verified its anti-apoptotic effects. The caspase family is the executor of apoptosis, leading to cellular structural damage and functional loss, and ultimately triggering apoptosis by cleaving key proteins within the cell. hNSC-Exos significantly reduced the expression of Caspase3 and increased the expression of Cleaved caspase3 in MCAO rats. We comprehensively evaluated from multiple angles that hNSC-Exos reversed neuronal apoptosis in MCAO rats. At the same time, we also observed the reversal of neurons by hNSC-Exos in vitro and validated this through multiple methods.

Neurons are the primary cell type in which extensive mitophagy is activated after ischemia, which may be an attempt to eliminate damaged mitochondria in a short period of time. Compared to the ischemic phase, neurons further increase mitophagy after reperfusion, which may be influenced by the OS environment [62]. Studies have shown that mtROS generated by ischemic injury induce the activation of mitophagy through various signaling pathways [63, 64]. Mitophagy mitigates OS damage by degrading and recycling damaged mitochondria, thereby maintaining the normal physiological activities of cells [65]. When mitophagy fails to eliminate OS, it triggers a series of apoptotic responses to protect the quality and function of mitochondria and regulate key processes in cell fate [66]. Therefore, enhancing mitophagy can be considered a novel therapeutic strategy for protecting ischemic neurons. Activated mitophagy includes multiple pathways, commonly involving the PINK1/Parkin-dependent pathway, receptor-mediated pathways (such as BNIP3, NIX, FUNDC1), and other non-classical pathways. Although these different pathways all play regulatory roles within the cell, BNIP3, NIX, and FUNDC1 are less specific and less finely regulated compared to PINK1/Parkin. Based on the above, we conducted a comprehensive preclinical study at the level of autophagy to further investigate whether hNSC-Exos are involved in the occurrence of mitophagy during CIRI and how this process mediates the recovery of neuronal function. RNA-seq analysis revealed increased lysosomal gene expression in OS-treated neurons, suggesting a role for lysosomes in mitophagy activation. To validate this result, we performed qRT-PCR to detect the expression levels of lysosomal genes with significant statistical significance from the sequencing results, all suggesting an increase in OS-induced neuron lysosome expression. Previous studies have supported that lysosomes with storage function dysregulation are associated with an early burst of autophagy [67]. Lysosomes play a significant role by fusing with autophagosomes to form autolysosomes, which degrade mitochondrial components. This sequencing result, to some extent, suggests the phenomenon of mitophagy under OS-induced models [66]. We further investigated the effect of exosomes-therapy on the regulation of mitophagy in damaged neuronal cells stimulated by OS. Using fluorescent dye MDC, TEM, and mCherry-GFP-LC3 dual fluorescence staining to detect the formation of autophagosome, we confirmed that hNSC-Exos further promoted mitophagy to eliminate OS-induced mitochondrial-dependent neuronal apoptosis. Additionally, the expression levels of mitophagy markers, such as Beclin and LC3B, increased, while the expression levels of neuronal apoptosis markers, such as Bax and Caspase 3, decreased. Combining the experimental results of this study with previous research [68], we believe that the expression changes of LC3A are significant, which would affect the trend of LC3B/LC3A. Therefore, LC3B/internal reference is more reflective of changes in autophagy. Interestingly, we confirmed the main pathway of mitophagy, which is the most extensively studied and can accurately identify damaged mitochondria, the PINK1/Parkin signaling pathway. When CIRI occurs, as neurons undergo apoptosis induced by OS, PINK1 senses mitochondrial membrane potential depolarization and accumulates on the mitochondrial surface, ubiquitinating proteins on the OMM, which are then further phosphorylated by PINK1. This aligns with previous studies, where overexpression of PINK1 significantly improved mitochondrial integrity in oxygen–glucose deprivation neurons [39]. Based on this research background, hNSC-Exos primarily exert their regulatory effect on mitophagy through this signaling pathway, thereby inhibiting the increase in intracellular ROS levels and apoptosis. Whether treated with the mitophagy inhibitor mdivi-1 or with PINK1 gene knockout, the therapeutic efficacy of hNSC-Exos showed a trend of weakening. Mdivi-1 is the first mitochondrial fission initiating protein selective kinase, which intensifies mtROS production and cell death by inhibiting mitochondrial fission, and weakens PINK1 mediated mitophagy. We validated the role of hNSC-Exos to some extent through the PINK1/Parkin pathway using mdivi-1 [69]. Next, we attempted to provide stronger evidence to validate the above results by establishing a PINK1 knockout cell model [70]. At the same time, in addition to hNSC-Exos regulating the global damage dominated by PINK1/Parkin, they may also target local damaged areas through the regulation of other different mitophagy pathways. For example, in non-classical mitophagy pathways,

OMM proteins mediate and cooperate with Parkin to enhance autophagic efficiency. When PINK1 is knocked out, partial functional compensation may be provided by other alternative mitophagy pathways. This includes BNIP3/NIX recruits autophagosomes directly through its LC3 interaction region (LIR domain), bypassing the PINK1/Parkin ubiquitination step [71]. In summary, this study indicates to some extent that hNSC-Exos promote mitophagy and reduce OS-induced damage in neurons.

It is worth noting that exosomes have been proven to transport proteins and RNA to recipient cells [72], triggering or inhibiting various signaling pathways associated with OS, apoptosis, and autophagy [73]. To our knowledge, this is the first detailed study on how hNSC-Exos reverse neuronal apoptosis through the mitophagy pathway, providing new insights for the clinical treatment of IS. However, this study's findings are preliminary and have some limitations. (1) Although this study focused on the relevant mechanisms during CIRI, it only examined short-term outcomes, lacking an assessment of the potential long-term benefits or risks of hNSC-Exos treatment. Future research should deeply evaluate the long-term efficacy and safety of hNSC-Exos in animal models [74]. (2) It remains unresolved how hNSC-Exos transmit signals and interact with damaged neurons by releasing bioactive molecules related to the PINK1/Parkin signaling pathway. It is essential to fully confirm the specific mechanisms by which hNSC-Exos regulate mitophagy among the numerous complex molecular components they carry. (3) We found that hNSC-Exos-promoted mitophagy protects damaged neural cells to a certain extent, but we have not conducted in-depth research on whether excessive autophagy stimulation accelerates ischemic brain injury [75, 76]. Various factors can affect the mitophagy' receptors, efficiency, lysosomal function, etc., in ischemic neurons, which requires a comprehensive observation and evaluation with the interaction and regulation of multiple variables. (4) Evidence supporting the regulation of mitophagy by exosomes mostly comes from animal studies [33, 77, 78], and human-related research is needed to confirm the experimental results. (5) The nature of the study is to move from preclinical research to clinical application, therefore, standardizing the source, production process, and biological composition of hNSC-Exos is essential. For example, selecting induced pluripotent stem cell (iPSC)-derived hNSCs as the cell source to ensure quality, classifying different vesicle subpopulations to ensure stability, and then optimizing the production process and establishing a strict quality control system for large-scale production to meet the needs of clinical applications [79]. Although the role of mitophagy in IS is complex and its specific mechanisms require in-depth study, we believe that uncovering the interaction and regulatory mechanisms between hNSC-Exos and PINK1/Parkin will provide new insights and potential therapeutic targets for the molecular biology mechanisms of mitophagy in IS.

Conclusion

In summary, this study demonstrates that hNSC-Exos represent a promising therapeutic approach for targeting mitochondrial dysfunction and reducing neuronal apoptosis during CIRI. By modulating the PINK1/Parkin mitophagy pathway, hNSC-Exos enhance neuronal repair and mitigate OS-induced damage. As a cell-free therapy, hNSC-Exos offer distinct advantages, including reduced immunogenicity and tumorigenicity, over traditional stem cell-based therapies. While these findings provide valuable insights into the mechanisms underlying hNSC-Exos-mediated neuroprotection, the study is limited by its reliance on preclinical models and short-term outcomes. Future research should focus on elucidating the molecular cargo of hNSC-Exos, optimizing their delivery, and validating their long-term efficacy and safety in human trials. These efforts will be critical to translating this promising therapy into clinical practice for IS and other neurological diseases characterized by mitochondrial dysfunction.

Abbreviations

Pathological terms

OS	Oxidative stress, an imbalance between the production of ROS and the antioxidant defenses of cells
IS	Ischemic stroke, a condition caused by obstruction of blood flow to the brain
CNS	Central nervous system, the main part of the nervous system, composed of the brain and spinal cord
ROS	Reactive oxygen species, chemically reactive molecules derived from oxygen, contributing to oxidative stress
CIRI	Cerebral ischemia/reperfusion injury, a secondary injury caused by the restoration of blood supply to ischemic brain tissue
AD	Alzheimer's disease, a neurodegenerative disorder characterized by memory loss and cognitive decline
PD	Parkinson's disease, a neurodegenerative disorder characterized by motor dysfunction and loss of dopaminergic neurons
TBI	Traumatic brain injury, damage to the brain caused by an external force, leading to cognitive, motor, or behavioral impairments
MtROS	Mitochondrial reactive oxygen species, a subset of ROS originating from mitochondria, implicated in neuronal damage

Biological molecules and structures

hNSCs	Human neural stem cells, progenitor cells capable of differentiating into various neural lineages
MSC	Mesenchymal stem cell, a multipotent stromal cell capable of differentiating into various cell types
ESCs	Embryonic stem cells, isolated from early embryos or primitive gonads and possess the characteristics of in vitro culture, unlimited proliferation, self-renewal, and multi-directional differentiation
hNSC-Exos	Human neural stem cell-derived exosomes, small extracellular vesicles secreted by hNSCs with neuroprotective properties
PINK1	PTEN-induced kinase 1, a key regulator of mitophagy in mitochondrial quality control which activates Parkin for mitochondrial clearance
BBB	Blood–brain barrier, a selective barrier that protects the brain from harmful substances in the blood

Drp1	Dynamin-related protein 1, a key regulator of mitochondrial fission
OPA1	Oxidative optic atrophy type 1, a protein involved in mitochondrial fusion and cristae structure maintenance
IMM	Inner mitochondrial membrane, the site of the electron transport chain and ATP synthesis
OMM	Outer mitochondrial membrane, the first barrier of mitochondria, interacting with cytosolic factors
CRISPR	Clustered regularly interspaced short palindromic repeats, a genome-editing technology
Cas9	CRISPR-associated protein 9, an enzyme used in CRISPR-Cas9 genome editing

Experimental techniques and models

MCAO	Middle cerebral artery occlusion, an experimental model for ischemic stroke in rats
WB	Western blotting, a technique for detecting specific proteins
qRT-PCR	quantitative real time PCR, a method for quantifying gene expression levels
RNA-seq	RNA sequencing, a high-throughput method for analyzing gene expression
TEM	Transmission electron microscopy, a high-resolution, high-magnification microscope for observing ultrastructures
MDC	Monodansylcadaverine, a fluorescent dye used to detect autophagic vacuoles
SD rats	Sprague Dawley rats, a common strain of laboratory rats used in research
DMEM	Dulbecco's modified eagle medium, a cell culture medium used for growing mammalian cells
PBS	Phosphate buffered saline, a buffer solution commonly used in biological experiments
NTA	Nanoparticle tracking analysis, a technique for measuring the size and concentration of extracellular vesicles
DAPI	4′,6-Diamidino-2-Phenylindole, a fluorescent stain for DNA used in microscopy
LDH	Lactate dehydrogenase, an enzyme used as a marker of cytotoxicity
TUNEL	TdT-mediated dUTP Nick End Labeling, a technique for detecting DNA fragmentation during apoptosis
HBSS	Hank's balanced salt solution, a buffer used for maintaining cell viability
GSEA	Gene set enrichment analysis, a method for identifying biological pathways enriched in differentially expressed genes
CCA	Common carotid artery, a major blood vessel supplying the head and neck
ECA	External carotid artery, a branch of the common carotid artery supplying the face and neck
ICA	Internal carotid artery, a branch of the common carotid artery supplying the brain
mNSS	Modified neurological severity score, a system for evaluating motor, sensory, and balance functions in ischemic stroke models
TTC	Triphenyltetrazolium ammonium chloride, a stain used to assess tissue viability
ANOVA	One-way analysis of variance, a statistical method for comparing means across multiple groups
SNK	Student–Newman–Keuls, a post-hoc statistical test used after ANOVA
LSD	Least significant difference, a statistical method for comparing group means
NMDA	N-methyl-D-aspartic acid, a receptor for glutamate involved in synaptic plasticity and memory
AMPA	α-Amino-3-hydroxy-5-methyl-4-isoxazolepropionic acid, a receptor for glutamate involved in fast synaptic transmission
NPCs	Neural progenitor cells, cells capable of differentiating into neurons and glia
GPCs	Glial progenitor cells, cells capable of differentiating into glial cells

Supplementary Information

The online version contains supplementary material available at https://doi.org/10.1186/s12967-025-06283-y.

Additional file 1.

Additional file 2.

Additional file 3.

Additional file 4.

Acknowledgements
We would like to thank Wiley Editing Services (https://wileyeditingservices.com) for English language editing.

Artificial Intelligence (AI)
The authors declare that they have not use AI-generated work in this manuscript.

Author contributions
MZ, JW, LW and JL conceived and designed research and performed experiments. SZ, SZ, CH, CT, YH and ZS analyzed data. MZ, JW and SZ prepared figures and edited text. MZ and JW drafted manuscript, LW and JL edited and revised manuscript. LW and JL gave final approval of the version to be published. All authors approved to submit this version to this publication.

Funding
The authors acknowledge the financial support received from the Program: Dalian Science and Technology Talent Innovation Support Policy Implementation Plan High-level Talent Team under Grant No. 2022RG18; National Nature Science Foundation of China under Grant No. 82072953; Dalian Outstanding Young Talents Project under Grant No. 2021RJ12; Dalian Young Science and Technology Stars Talent Program under Grant No.2024RQ011; Liaoning Province Science and Technology Plan Joint Program Talent Project under Grant No. 2024-MSLH-116; Liaoning Province Science and Technology Plan Joint Program Talent Project under Grant No. 2024-BSLH-053; Doctoral Scientific Startup Fund of Liaoning Province under Grant No.2023-BS-159.

Availability of data and materials
The original data applied in this research are accessible from the corresponding author.

Declarations

Ethics approval and consent to participate
Human neural stem cell was obtained from the human fetal forebrain tissue of healthy pregnant women at 10–12 weeks of gestation who requested induced abortion, all of whom provided informed consent and tested negative for pathogenic microorganisms. All procedures were approved by the Clinical Research Ethics Committee of the First Affiliated Hospital of Dalian Medical University (Approved project: Clinical research of neural stem cells, Approval No. LCKY2016-60, Approval date: Dec. 2nd 2016), and complied with the standards of the National Health Research Institute. The experiments conducted on animals were approved by the Ethics Committee of the Animal Experiment Center of Dalian Medical University and performed following the Guide for the Care and Use of Laboratory Animals of the National Institutes of Health (Approved project: Study on the repair of neurological damage in ischemic stroke by engineered neural stem cell vesicles, Approval No. AEE23127, Approval date: Feb. 28th 2023). Methods for each procedure were performed in accordance with the approved guidelines and regulations. All experiments were conducted in compliance with the ARRIVE guidelines.

Consent for publication
Not applicable.

Competing interests
The authors declare no competing financial interest.

Author details
[1]Stem Cell Clinical Research Center, The First Affiliated Hospital of Dalian Medical University, No. 193, Lianhe Road, Shahekou District, Dalian 116011, People's Republic of China. [2]National Local Joint Engineering Laboratory, The First Affiliated Hospital of Dalian Medical University, No. 193, Lianhe Road, Shahekou District, Dalian 116011, People's Republic of China. [3]National Genetic Test Center, The First Affiliated Hospital of Dalian Medical University, No. 193, Lianhe Road, Shahekou District, Dalian 116011, People's Republic of China. [4]Liaoning Key Laboratory of Frontier Technology of Stem Cell and Precision Medicine, Dalian Innovation Institute of Stem Cell and Precision Medicine, No. 57, Xinda Street, High-Tech Park, Dalian 116023, People's Republic of China.

Received: 25 November 2024 Accepted: 20 February 2025
Published online: 05 April 2025

References

1. Picard M, Shirihai OS. Mitochondrial signal transduction. Cell Metab. 2022;34(11):1620–53.
2. Iadecola C, Anrather J. The immunology of stroke: from mechanisms to translation. Nat Med. 2011;17(7):796–808.
3. Naito MG, Xu D, Amin P, Lee J, Wang H, Li W, Kelliher M, Pasparakis M, Yuan J. Sequential activation of necroptosis and apoptosis cooperates to mediate vascular and neural pathology in stroke. Proc Natl Acad Sci USA. 2020;117(9):4959–70.
4. Zhao M, Wang J, Zhu S, Wang M, Chen C, Wang L, Liu J. Mitochondrion-based organellar therapies for central nervous system diseases. Cell Communication and Signaling. 2024;22(1):487.
5. Moskowitz MA, Lo EH, Iadecola C. The science of stroke: mechanisms in search of treatments. Neuron. 2010;67(2):181–98.
6. Huang L, Wong S, Snyder EY, Hamblin MH, Lee JP. Human neural stem cells rapidly ameliorate symptomatic inflammation in early-stage ischemic-reperfusion cerebral injury. Stem Cell Res Ther. 2014;5(6):129.
7. Wang S, He Q, Qu Y, Yin W, Zhao R, Wang X, Yang Y, Guo ZN. Emerging strategies for nerve repair and regeneration in ischemic stroke: neural stem cell therapy. Neural Regen Res. 2024;19(11):2430–43.
8. Gu N, Rao C, Tian Y, Di Z, Liu Z, Chang M, Lei H. Anti-inflammatory and antiapoptotic effects of mesenchymal stem cells transplantation in rat brain with cerebral ischemia. J Stroke Cerebrovasc Dis. 2014;23(10):2598–606.
9. Wei L, Cui L, Snider BJ, Rivkin M, Yu SS, Lee CS, Adams LD, Gottlieb DI, Johnson EM Jr, Yu SP, et al. Transplantation of embryonic stem cells overexpressing Bcl-2 promotes functional recovery after transient cerebral ischemia. Neurobiol Dis. 2005;19(1–2):183–93.
10. Chen L, Zhang G, Gu Y, Guo X. Meta-analysis and systematic review of neural stem cells therapy for experimental ischemia stroke in preclinical studies. Sci Rep. 2016;6:32291.
11. Jiao Y, Liu YW, Chen WG, Liu J. Neuroregeneration and functional recovery after stroke: advancing neural stem cell therapy toward clinical application. Neural Regen Res. 2021;16(1):80–92.
12. Zhu ZH, Jia F, Ahmed W, Zhang GL, Wang H, Lin CQ, Chen WH, Chen LK. Neural stem cell-derived exosome as a nano-sized carrier for BDNF delivery to a rat model of ischemic stroke. Neural Regen Res. 2023;18(2):404–9.
13. Li X, Fang P, Mai J, Choi ET, Wang H, Yang XF. Targeting mitochondrial reactive oxygen species as novel therapy for inflammatory diseases and cancers. J Hematol Oncol. 2013;6:19.
14. Wang HX, Liu C, Li YY, Cao Y, Zhao L, Zhao YJ, Deng ZA, Tong AP, Zhou LX. TUG-891 inhibits neuronal endoplasmic reticulum stress and pyroptosis activation and protects neurons in a mouse model of intraventricular hemorrhage. Neural Regen Res. 2023;18(10):2278–84.
15. Tan MS, Tan L, Jiang T, Zhu XC, Wang HF, Jia CD, Yu JT. Amyloid-β induces NLRP1-dependent neuronal pyroptosis in models of Alzheimer's disease. Cell Death Dis. 2014;5(8):e1382.
16. Fan Y, Chen Z, Zhang M. Role of exosomes in the pathogenesis, diagnosis, and treatment of central nervous system diseases. J Transl Med. 2022;20(1):291.
17. Youle RJ, Narendra DP. Mechanisms of mitophagy. Nat Rev Mol Cell Biol. 2011;12(1):9–14.
18. Jia J, Jin H, Nan D, Yu W, Huang Y. New insights into targeting mitochondria in ischemic injury. Apoptosis. 2021;26(3–4):163–83.
19. Guan R, Zou W, Dai X, Yu X, Liu H, Chen Q, Teng W. Mitophagy, a potential therapeutic target for stroke. J Biomed Sci. 2018;25(1):87.
20. Chu CT. Eaten alive: autophagy and neuronal cell death after hypoxia-ischemia. Am J Pathol. 2008;172(2):284–7.
21. Kubli DA, Gustafsson ÅB. Mitochondria and mitophagy: the yin and yang of cell death control. Circ Res. 2012;111(9):1208–21.
22. Shi RY, Zhu SH, Li V, Gibson SB, Xu XS, Kong JM. BNIP3 interacting with LC3 triggers excessive mitophagy in delayed neuronal death in stroke. CNS Neurosci Ther. 2014;20(12):1045–55.
23. Bellot G, Garcia-Medina R, Gounon P, Chiche J, Roux D, Pouysségur J, Mazure NM. Hypoxia-induced autophagy is mediated through hypoxia-inducible factor induction of BNIP3 and BNIP3L via their BH3 domains. Mol Cell Biol. 2009;29(10):2570–81.
24. Narendra DP, Youle RJ. The role of PINK1-Parkin in mitochondrial quality control. Nat Cell Biol. 2024;26(10):1639–51.
25. Valente EM, Salvi S, Ialongo T, Marongiu R, Elia AE, Caputo V, Romito L, Albanese A, Dallapiccola B, Bentivoglio AR. PINK1 mutations are associated with sporadic early-onset parkinsonism. Ann Neurol. 2004;56(3):336–41.
26. Yang Y, Ouyang Y, Yang L, Beal MF, McQuibban A, Vogel H, Lu B. Pink1 regulates mitochondrial dynamics through interaction with the fission/fusion machinery. Proc Natl Acad Sci USA. 2008;105(19):7070–5.
27. Zuo W, Zhang S, Xia CY, Guo XF, He WB, Chen NH. Mitochondria autophagy is induced after hypoxic/ischemic stress in a Drp1 dependent manner: the role of inhibition of Drp1 in ischemic brain damage. Neuropharmacology. 2014;86:103–15.
28. Zeng Z, You M, Fan C, Rong R, Li H, Xia X. Pathologically high intraocular pressure induces mitochondrial dysfunction through Drp1 and leads to retinal ganglion cell PANoptosis in glaucoma. Redox Biol. 2023;62:102687.
29. Sekine S. PINK1 import regulation at a crossroad of mitochondrial fate: the molecular mechanisms of PINK1 import. J Biochem. 2020;167(3):217–24.
30. Wen H, Li L, Zhan L, Zuo Y, Li K, Qiu M, Li H, Sun W, Xu E. Hypoxic postconditioning promotes mitophagy against transient global cerebral ischemia via PINK1/Parkin-induced mitochondrial ubiquitination in adult rats. Cell Death Dis. 2021;12(7):630.
31. Redmann M, Dodson M, Boyer-Guittaut M, Darley-Usmar V, Zhang J. Mitophagy mechanisms and role in human diseases. Int J Biochem Cell Biol. 2014;53:127–33.
32. Lei L, Yang S, Lu X, Zhang Y, Li T. Research progress on the mechanism of mitochondrial autophagy in cerebral stroke. Front Aging Neurosci. 2021;13:698601.
33. Zhang L, Lin Y, Bai W, Sun L, Tian M. Human umbilical cord mesenchymal stem cell-derived exosome suppresses programmed cell death in traumatic brain injury via PINK1/Parkin-mediated mitophagy. CNS Neurosci Ther. 2023;29(8):2236–58.
34. Lai TC, Lee TL, Chang YC, Chen YC, Lin SR, Lin SW, Pu CM, Tsai JS, Chen YL. MicroRNA-221/222 mediates ADSC-exosome-induced cardioprotection against ischemia/reperfusion by targeting PUMA and ETS-1. Front Cell Dev Biol. 2020;8:569150.
35. Chen G, Wang M, Ruan Z, Zhu L, Tang C. Mesenchymal stem cell-derived exosomal miR-143-3p suppresses myocardial ischemia-reperfusion injury by regulating autophagy. Life Sci. 2021;280:119742.
36. Jiang M, Wang H, Jin M, Yang X, Ji H, Jiang Y, Zhang H, Wu F, Wu G, Lai X, et al. Exosomes from MiR-30d-5p-ADSCs reverse acute ischemic stroke-induced, autophagy-mediated brain injury by promoting M2 microglial/macrophage polarization. Cell Physiol Biochem. 2018;47(2):864–78.
37. Zhao ZY, Luan P, Huang SX, Xiao SH, Zhao J, Zhang B, Gu BB, Pi RB, Liu J. Edaravone protects HT22 neurons from H2O2-induced apoptosis by inhibiting the MAPK signaling pathway. CNS Neurosci Ther. 2013;19(3):163–9.
38. Lv Z, Li Y, Wang Y, Cong F, Li X, Cui W, Han C, Wei Y, Hong X, Liu Y, et al. Safety and efficacy outcomes after intranasal administration of neural stem cells in cerebral palsy: a randomized phase 1/2 controlled trial. Stem Cell Res Ther. 2023;14(1):23.
39. Wang J, Zhao M, Wang M, Fu D, Kang L, Xu Y, Shen L, Jin S, Wang L, Liu J. Human neural stem cell-derived artificial organelles to improve oxidative phosphorylation. Nat Commun. 2024;15(1):7855.
40. Cheng X, Yang YL, Li WH, Liu M, Wang YH, Du GH. Cerebral ischemia-reperfusion aggravated cerebral infarction injury and possible differential genes identified by RNA-Seq in rats. Brain Res Bull. 2020;156:33–42.

41. Ye YC, Chang ZH, Wang P, Wang YW, Liang J, Chen C, Wang JJ, Sun HT, Wang Y, Li XH. Infarct-preconditioning exosomes of umbilical cord mesenchymal stem cells promoted vascular remodeling and neurological recovery after stroke in rats. Stem Cell Res Ther. 2022;13(1):378.
42. Chen J, Li Y, Wang L, Zhang Z, Lu D, Lu M, Chopp M. Therapeutic benefit of intravenous administration of bone marrow stromal cells after cerebral ischemia in rats. Stroke. 2001;32(4):1005–11.
43. Théry C, Witwer KW, Aikawa E, Alcaraz MJ, Anderson JD, Andriantsitohaina R, Antoniou A, Arab T, Archer F, Atkin-Smith GK, et al. Minimal information for studies of extracellular vesicles 2018 (MISEV2018): a position statement of the international society for extracellular vesicles and update of the MISEV2014 guidelines. J Extracell Vesicles. 2018;7(1):1535750.
44. Qin C, Yang S, Chu YH, Zhang H, Pang XW, Chen L, Zhou LQ, Chen M, Tian DS, Wang W. Signaling pathways involved in ischemic stroke: molecular mechanisms and therapeutic interventions. Signal Transduct Target Ther. 2022;7(1):215.
45. Zhu Z, Zhang Q, Feng J, Zebaze Dongmo S, Zhang Q, Huang S, Liu X, Zhang G, Chen L. Neural stem cell-derived small extracellular vesicles: key players in ischemic stroke therapy - a comprehensive literature review. Int J Nanomed. 2024;19:4279–95.
46. Qin T, Li C, Xu Y, Qin Y, Jin Y, He R, Luo Z, Zhao J, Duan C, Lu H, et al. Local delivery of EGFR(+)NSCs-derived exosomes promotes neural regeneration post spinal cord injury via miR-34a-5p/HDAC6 pathway. Bioactive Mater. 2024;33:424–43.
47. Ballabio A, Bonifacino JS. Lysosomes as dynamic regulators of cell and organismal homeostasis. Nat Rev Mol Cell Biol. 2020;21(2):101–18.
48. Sun Y, Li M, Zhao D, Li X, Yang C, Wang X. Lysosome activity is modulated by multiple longevity pathways and is important for lifespan extension in C. elegans. eLife. 2020;9:e55745.
49. Yang C, Wang X. Lysosome biogenesis regulation and functions. J Cell Biol. 2021;220(6):e202102001.
50. Allen CL, Bayraktutan U. Oxidative stress and its role in the pathogenesis of ischaemic stroke. Int J Stroke. 2009;4(6):461–70.
51. Webb RL, Kaiser EE, Jurgielewicz BJ, Spellicy S, Scoville SL, Thompson TA, Swetenburg RL, Hess DC, West FD, Stice SL. Human neural stem cell extracellular vesicles improve recovery in a porcine model of ischemic stroke. Stroke. 2018;49(5):1248–56.
52. Farzaneh M, Khoshnam SE. Functional roles of mesenchymal stem cell-derived exosomes in ischemic stroke treatment. Curr Stem Cell Res Ther. 2024;19(1):2–14.
53. Kobayashi S, Fukuma S, Ikenoue T, Fukuhara S, Kobayashi S. Effect of edaravone on neurological symptoms in real-world patients with acute ischemic stroke. Stroke. 2019;50(7):1805–11.
54. Wang A, Jia B, Zhang X, Huo X, Chen J, Gui L, Cai Y, Guo Z, Han Y, Peng Z, et al. Efficacy and safety of butylphthalide in patients with acute ischemic stroke: a randomized clinical trial. JAMA Neurol. 2023;80(8):851–9.
55. Tatsuta T, Langer T. Quality control of mitochondria: protection against neurodegeneration and ageing. EMBO J. 2008;27(2):306–14.
56. Jin Z, Wu J, Yan LJ. Chemical conditioning as an approach to ischemic stroke tolerance: mitochondria as the target. Int J Mol Sci. 2016;17(3):351.
57. Li M, Tang H, Li Z, Tang W. Emerging treatment strategies for cerebral ischemia-reperfusion injury. Neuroscience. 2022;507:112–24.
58. Karnas E, Dudek P, Zuba-Surma EK. Stem cell- derived extracellular vesicles as new tools in regenerative medicine - immunomodulatory role and future perspectives. Front Immunol. 2023;14:1120175.
59. Caponnetto F, Manini I, Skrap M, Palmai-Pallag T, Di Loreto C, Beltrami AP, Cesselli D, Ferrari E. Size-dependent cellular uptake of exosomes. Nanomedicine. 2017;13(3):1011–20.
60. Cetin A, Komai S, Eliava M, Seeburg PH, Osten P. Stereotaxic gene delivery in the rodent brain. Nat Protoc. 2006;1(6):3166–73.
61. Wang J, Zhao M, Fu D, Wang M, Han C, Lv Z, Wang L, Liu J. Human neural stem cell-derived extracellular vesicles protect against ischemic stroke by activating the PI3K/AKT/mTOR pathway. Neural Regen Res. 2025;20(11):3245–58.
62. Xiao B, Deng X, Lim GGY, Xie S, Zhou ZD, Lim KL, Tan EK. Superoxide drives progression of Parkin/PINK1-dependent mitophagy following translocation of Parkin to mitochondria. Cell Death Dis. 2017;8(10):e3097.
63. Mao Z, Tian L, Liu J, Wu Q, Wang N, Wang G, Wang Y, Seto S. Ligustilide ameliorates hippocampal neuronal injury after cerebral ischemia reperfusion through activating PINK1/Parkin-dependent mitophagy. Phytomedicine. 2022;101:154111.
64. Xiao B, Goh JY, Xiao L, Xian H, Lim KL, Liou YC. Reactive oxygen species trigger Parkin/PINK1 pathway-dependent mitophagy by inducing mitochondrial recruitment of Parkin. J Biol Chem. 2017;292(40):16697–708.
65. Fan P, Xie XH, Chen CH, Peng X, Zhang P, Yang C, Wang YT. Molecular regulation mechanisms and interactions between reactive oxygen species and mitophagy. DNA Cell Biol. 2019;38(1):10–22.
66. Wang S, Long H, Hou L, Feng B, Ma Z, Wu Y, Zeng Y, Cai J, Zhang DW, Zhao G. The mitophagy pathway and its implications in human diseases. Signal Transduct Target Ther. 2023;8(1):304.
67. Zhang X, Wei M, Fan J, Yan W, Zha X, Song H, Wan R, Yin Y, Wang W. Ischemia-induced upregulation of autophagy preludes dysfunctional lysosomal storage and associated synaptic impairments in neurons. Autophagy. 2021;17(6):1519–42.
68. Nieto-Torres JL, Shanahan SL, Chassefeyre R, Chaiamarit T, Zaretski S, Landeras-Bueno S, Verhelle A, Encalada SE, Hansen M. LC3B phosphorylation regulates FYCO1 binding and directional transport of autophagosomes. Curr Biol. 2021;31(15):3440-3449.e3447.
69. Fan Y, Cheng Z, Mao L, Xu G, Li N, Zhang M, Weng P, Zheng L, Dong X, Hu S, et al. PINK1/TAX1BP1-directed mitophagy attenuates vascular endothelial injury induced by copper oxide nanoparticles. J Nanobiotechnol. 2022;20(1):149.
70. Zhang S, Shen J, Li D, Cheng Y. Strategies in the delivery of Cas9 ribonucleoprotein for CRISPR/Cas9 genome editing. Theranostics. 2021;11(2):614–48.
71. Marinković M, Šprung M, Novak I. Dimerization of mitophagy receptor BNIP3L/NIX is essential for recruitment of autophagic machinery. Autophagy. 2021;17(5):1232–43.
72. Kalluri R, LeBleu VS. The biology, function and biomedical applications of exosomes. Science. 2020;367:6478.
73. Mathieu M, Martin-Jaular L, Lavieu G, Théry C. Specificities of secretion and uptake of exosomes and other extracellular vesicles for cell-to-cell communication. Nat Cell Biol. 2019;21(1):9–17.
74. Ajoolabady A, Wang S, Kroemer G, Penninger JM, Uversky VN, Pratico D, Henninger N, Reiter RJ, Bruno A, Joshipura K, et al. Targeting autophagy in ischemic stroke: from molecular mechanisms to clinical therapeutics. Pharmacol Ther. 2021;225:107848.
75. Li YY, Qin ZH, Sheng R. The multiple roles of autophagy in neural function and diseases. Neurosci Bull. 2024;40(3):363–82.
76. Moloudizargari M, Asghari MH, Ghobadi E, Fallah M, Rasouli S, Abdollahi M. Autophagy, its mechanisms and regulation: implications in neurodegenerative diseases. Ageing Res Rev. 2017;40:64–74.
77. Li N, Shu J, Yang X, Wei W, Yan A. Exosomes derived from M2 microglia cells attenuates neuronal impairment and mitochondrial dysfunction in alzheimer's disease through the PINK1/Parkin pathway. Front Cell Neurosci. 2022;16:874102.
78. Sheng B, Gao S, Chen X, Liu Y, Lai N, Dong J, Sun J, Zhou Y, Wu L, Hang CH, et al. Exosomes-mediated delivery of miR-486–3p alleviates neuroinflammation via SIRT2-mediated inhibition of mitophagy after subarachnoid hemorrhage. Stroke Vasc Neurol. https://doi.org/10.1136/svn-2024-003509.
79. Rezaie J, Feghhi M, Etemadi T. A review on exosomes application in clinical trials: perspective, questions, and challenges. Cell Commun Signal. 2022;20(1):145.

Publisher's Note